Comparison of lidar-derived PM10 with regional modeling and ground-based observations in the frame of MEGAPOLI experiment

P. Royer, P. Chazette, K. Sartelet, Q. J. Zhang, Matthias Beekmann, Jean-Christophe Raut

Atmos. Chem. Phys., 11, 10705–10726, 2011
www.atmos-chem-phys.net/11/10705/2011/
doi:10.5194/acp-11-10705-2011

Atmospheric Chemistry and Physics

Comparison of lidar-derived PM_{10} with regional modeling and ground-based observations in the frame of MEGAPOLI experiment

P. Royer[1,2], P. Chazette[1], K. Sartelet[3], Q. J. Zhang[4,5], M. Beekmann[4], and J.-C. Raut[6]

[1]Laboratoire des Sciences du Climat et de l'Environnement (LSCE), Laboratoire mixte CEA-CNRS-UVSQ, UMR 1572, CEA Saclay, 91191 Gif-sur-Yvette, France
[2]LEOSPHERE, 76 rue de Monceau, 75008 Paris, France
[3]Centre d'Enseignement et de Recherche en Environnement Atmosphérique (CEREA), Joint Laboratory Ecole des Ponts Paris Tech/EDF R&D, Université Paris-Est, 6–8 Avenue Blaise Pascal, Cité Descartes Champs-sur-Marne, 77455 Marne la Vallée, France
[4]Laboratoire Inter-universitaire des Systèmes Atmosphériques (LISA), Laboratoire mixte Paris VII-UPEC-CNRS, UMR 7583, 61 Avenue du Général de Gaulle, 94010 Créteil, France
[5]ARIA Technologies, 8–10 rue de la ferme, 92100, Boulogne-Billancourt, France
[6]Laboratoire Atmosphères Milieux Observations Spatiales (LATMOS), Laboratoire mixte UPMC-UVSQ-CNRS, UMR 8190, Université Paris 6, 4 Place Jussieu, 75252 Paris, France

Received: 8 March 2011 – Published in Atmos. Chem. Phys. Discuss.: 15 April 2011
Revised: 9 August 2011 – Accepted: 20 September 2011 – Published: 28 October 2011

Abstract. An innovative approach using mobile lidar measurements was implemented to test the performances of chemistry-transport models in simulating mass concentrations (PM_{10}) predicted by chemistry-transport models. A ground-based mobile lidar (GBML) was deployed around Paris onboard a van during the MEGAPOLI (Megacities: Emissions, urban, regional and Global Atmospheric POLlution and climate effects, and Integrated tools for assessment and mitigation) summer experiment in July 2009. The measurements performed with this Rayleigh-Mie lidar are converted into PM_{10} profiles using optical-to-mass relationships previously established from in situ measurements performed around Paris for urban and peri-urban aerosols. The method is described here and applied to the 10 measurements days (MD). MD of 1, 15, 16 and 26 July 2009, corresponding to different levels of pollution and atmospheric conditions, are analyzed here in more details. Lidar-derived PM_{10} are compared with results of simulations from POLYPHEMUS and CHIMERE chemistry-transport models (CTM) and with ground-based observations from the AIRPARIF network. GBML-derived and AIRPARIF in situ measurements have been found to be in good agreement with a mean Root Mean Square Error RMSE (and a Mean Absolute Percentage Error MAPE) of 7.2 $\mu g\,m^{-3}$ (26.0 %) and 8.8 $\mu g\,m^{-3}$ (25.2 %) with relationships assuming peri-urban and urban-type particles, respectively. The comparisons between CTMs and lidar at ∼200 m height have shown that CTMs tend to underestimate wet PM_{10} concentrations as revealed by the mean wet PM_{10} observed during the 10 MD of 22.4, 20.0 and 17.5 $\mu g\,m^{-3}$ for lidar with peri-urban relationship, and POLYPHEMUS and CHIMERE models, respectively. This leads to a RMSE (and a MAPE) of 6.4 $\mu g\,m^{-3}$ (29.6 %) and 6.4 $\mu g\,m^{-3}$ (27.6 %) when considering POLYPHEMUS and CHIMERE CTMs, respectively. Wet integrated PM_{10} computed (between the ground and 1 km above the ground level) from lidar, POLYPHEMUS and CHIMERE results have been compared and have shown similar results with a RMSE (and MAPE) of 6.3 $mg\,m^{-2}$ (30.1 %) and 5.2 $mg\,m^{-2}$ (22.3 %) with POLYPHEMUS and CHIMERE when comparing with lidar-derived PM_{10} with periurban relationship. The values are of the same order of magnitude than other comparisons realized in previous studies. The discrepancies observed between models and measured PM_{10} can be explained by difficulties to accurately model the background conditions, the positions and strengths of the plume, the vertical turbulent diffusion (as well as the limited vertical model resolutions) and chemical processes as the formation of secondary aerosols. The major advantage of using vertically

Correspondence to: P. Royer
(philippe.royer@lsce.ipsl.fr)

Published by Copernicus Publications on behalf of the European Geosciences Union.

resolved lidar observations in addition to surface concentrations is to overcome the problem of limited spatial representativity of surface measurements. Even for the case of a well-mixed boundary layer, vertical mixing is not complete, especially in the surface layer and near source regions. Also a bad estimation of the mixing layer height would introduce errors in simulated surface concentrations, which can be detected using lidar measurements. In addition, horizontal spatial representativity is larger for altitude integrated measurements than for surface measurements, because horizontal inhomogeneities occurring near surface sources are dampened.

1 Introduction

Aerosol pollution studies in urban centers are of increasing interest as they directly concern almost half of the world's population. Moreover, urban population is expected to continue to increase during the next decades. Epidemiological studies have clearly established that small particles with an aerodynamic diameter below 2.5 µm ($PM_{2.5}$) and below 1 µm (PM_1), and mainly originating from traffic and industrial activities, have an impact on human health by penetrating the respiratory system and leading to respiratory (allergies, asthma, altered lung function) and cardiovascular diseases (e.g. Dockery and Pope, 1996; Lauwerys, 1982). The study of air quality in megacities, with often large particulate matter loads, and potentially large health impact is thus an important issue (e.g. Gurjar et al., 2008). In particular, it is still important to improve our understanding of physico-chemical, transport and emission processes that play a key role in the formation of pollution peaks within megacities and their surroundings. In addition, several studies have also shown that megacities have an important regional impact on air quality and climate (e.g. Lawrence et al., 2007).

The Paris agglomeration with about 12 millions of inhabitants is one of the three megacities in Europe (with London and Moscow). Air quality is continuously monitored over the agglomeration by a dedicated surface network (AIRPARIF, http://www.airparif.asso.fr/). Furthermore, aerosol chemical and optical properties over Paris have been investigated in the framework of several campaigns: ESQUIF in 1999 (Etude et Simulation de la QUalité de l'air en Ile de France; Vautard et al., 2003; Chazette et al., 2005), MEAUVE (Modélisation des Effets des Aérosols en Ultra Violet et Expérimentation) in 2001 (Lavigne et al., 2005), LISAIR (Lidar pour la Surveillance de l'AIR) in 2005 (Raut and Chazette, 2007) and ParisFog in 2007 (Elias et al., 2009; Haeffelin et al., 2010). Ground-based in-situ measurements in dry conditions performed during these campaigns gave the opportunity to determine optical-to-mass relationships for urban, peri-urban and rural environments over the Ile-de-France region (with Paris in its center) (Raut and Chazette, 2009).

Table 1. GBML main technical characteristics.

Laser	Nd:YAG 20 Hz 16 mJ @ 355 nm
Reception diameter	150 mm
Full overlap	150–200 m
Detector	Photomultiplier tubes
Filter bandwidth (FWHM)	0.3 nm
Data acquisition system	PXI 100 MHz
Raw/final resolution along the line of sight	1.5 m/15 m
Temporal resolution	20 s
Lidar head size	$\sim 65 \times 35 \times 18$ cm
Lidar head and electronics weight	~ 40 kg
Power supply	4 batteries (12 V, 75 A h^{-1})

In the frame of the FP7/MEGAPOLI project (seventh Framework Programme/Megacities: Emissions, urban, regional and Global Atmospheric POLlution and climate effects, and Integrated tools for assessment and mitigation; http://megapoli.dmi.dk/), an intensive campaign was organized in the Ile de France region in summer (July) 2009 and winter (15 January–15 February) 2010, in order to better quantify organic aerosol sources in a large megacity in temperate latitudes. A large ensemble of ground based measurements at three primary and several secondary sites, by mobile vans, and by aircraft has been set-up. Detailed measurements of aerosol chemical composition and physico-chemical properties, of gas phase chemistry and of meteorological variables were performed on these platforms. Campaign objectives and measurement set-up will be described in detail in a later paper in this special section. As part of this campaign, a ground-based mobile lidar (GBML) was deployed onboard a van in order to investigate the aerosol load and the evolution of aerosol optical properties in the urban plume.

We present here vertically-resolved PM_{10} (mass concentration of aerosols with an aerodynamic diameter lower than 10 µm) retrieved from GBML measurements performed during the MEGAPOLI campaign using optical-to-mass relationships previously established over the Paris region. In addition, a comparison with two regional chemical-transport models is performed. The next section (Sect. 2) details the experimental setup (instrumentation and observation strategy). The modeling approach is detailed in Sect. 3 as well as the commonalities and differences between the two CTMs. The methodology, uncertainties and results of lidar-derived PM_{10} are presented in Sect. 4 and compared to AIRPARIF measurements. Finally, CHIMERE and POLYPHEMUS CTMs simulations are compared to GBML-derived and AIRPARIF-measured PM_{10} (Sect. 5).

2 Experimental setup

2.1 Instrumentation

2.1.1 Ground-based mobile lidar

The ground based mobile lidar (GBML) used during the MEGAPOLI campaign is based on an ALS450® lidar commercialized by the LEOSPHERE company and initially developed by the Commissariat à l'Energie Atomique (CEA) and the Centre National de la Recherche Scientifique (CNRS) (Chazette et al., 2007). The main characteristics of this lidar are summarized in Table 1. It is based on an Ultra® Nd:Yag laser manufactured by Quantel company, delivering ∼6 ns width pulses at the repetition rate of 20 Hz with a mean pulse energy of 16 mJ at 355 nm. The acquisition is realized with a PCI eXtensions for Instrumentation (PXI®) system at 100 MHz (National Instruments). This compact (∼65 × 35 × 18 cm^3) and light (∼40 kg for the lidar head and electronics) instrument was taken onboard a van with a power supply delivered by 4 batteries (12 V, 75 A h^{-1}) giving an autonomy of ∼3 h 30 min. This system is particularly well-adapted to air pollution and tropospheric aerosol studies thanks to its full overlap reached at about 150–200 m height and its high vertical resolution of 1.5 m. The detection is realized with photomultiplier tubes and narrowband filters with a bandwidth of 0.3 nm. It gives access to the aerosol optical properties (depolarization ratio and extinction coefficient in synergy with sun-photometer measurements) and the atmospheric structures (planetary boundary layer (PBL) height, aerosol and cloud layers). The final vertical resolution of the data is 15 m after filtering for a temporal resolution of 20 s.

2.1.2 AIRPARIF network

AIRPARIF is the regional operational network in charge of air quality survey around the Paris area. It is composed of 68 stations spread out in a radius of 100 km around Paris measuring every hour critical gases and/or aerosol concentrations (PM_{10} and $PM_{2.5}$). Two different types of stations are distinguished: 26 stations close to the traffic sources and 42 background (urban, peri-urban or rural) stations. From the entire set of measurements (NO, NO_2, ozone, PM_{10}, other pollutants, depending on the site), we have only used here PM_{10} concentrations measurements performed with automatic TEOM instruments (Tapered Element Oscillating Microbalance, Pataschnik and Rupprecht, 1991). PM_{10} concentrations are regulated in France. Since 2005 the threshold values are 40 µg m^{-3} as an annual average and 50 µg m^{-3} as a daily average which must not to be exceeded on more than 35 days per year. The information and alert thresholds are respectively 80 and 125 µg m^{-3} in daily mean. The uncertainty on PM_{10} concentrations measured with a TEOM instrument has been assessed to be between 14.8 and 20.9 % (personal communication from AIRPARIF). It is noteworthy that TEOM measurements correspond to dry PM_{10} as sampling is performed through a warmed inlet at ∼50 °C. Figure 1 shows the localization of the 22 AIRPARIF stations measuring PM_{10} concentrations: 10 urban (green circles), 3 peri-urban (blue circles), 3 rural (cyan circles) and 6 traffic stations (red circles) according to AIRPARIF criteria. These latter are not considered in this study because they are not representative of background aerosol concentrations.

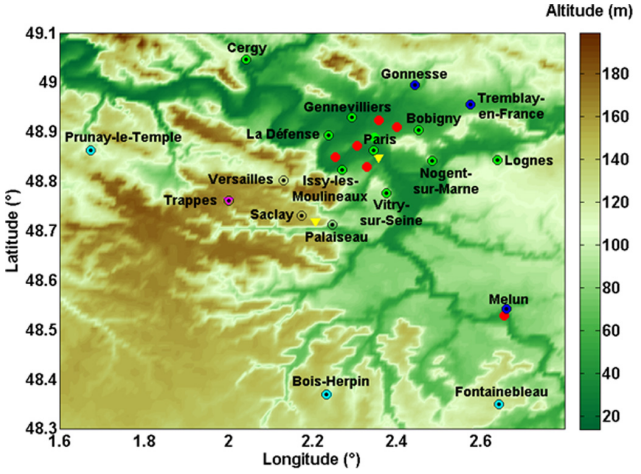

Fig. 1. Topographic map with the main cities in the vicinity of Paris. Colored circles indicate rural (in cyan), peri-urban (in blue), urban (in green) and traffic (in red) AIRPARIF stations measuring PM_{10}. Paris and Palaiseau AERONET sun-photometer stations and the location of Trappes radiosoundings are also indicated by yellow and pink triangles, respectively.

2.1.3 AERONET sun-photometer network

The AErosol RObotic NETwork (AERONET) is an automatic and global network of sun-photometers which provides long-term and continuous monitoring of aerosol optical, microphysical and radiative properties (http://aeronet.gsfc.nasa.gov/, Holben et al., 1998). Each site is composed of a 318A® sun and sky scanning spectral radiometer manufactured by CIMEL Electronique. For direct sun measurement eight spectral bands are used between 340 and 1020 nm. The five standard wavelengths are 440, 670, 870, 940 and 1020 nm. Aerosol Optical Depth (AOD) values are computed for three data quality levels: level 1.0 (unscreened), level 1.5 (cloud-screened), and level 2.0 (cloud screened and quality-assured). The total uncertainty on AOD is $< \pm 0.01$ for $\lambda >$ 440 nm and $< \pm 0.02$ for $\lambda < 440$ nm (Holben et al., 1998). Four AERONET sun-photometers are located within the Ile-de-France region, within the administrative boundaries of Paris and in the suburbs Palaiseau, Créteil and Fontainebleau sites. We only used in this study level 2.0 AOD data at 340, 380 and 440 nm from Paris (latitude 48.85° N; longitude 2.36° E; altitude 50 m) and Palaiseau (latitude 48.72° N; longitude 2.21° E; altitude 156 m) sun-photometers stations

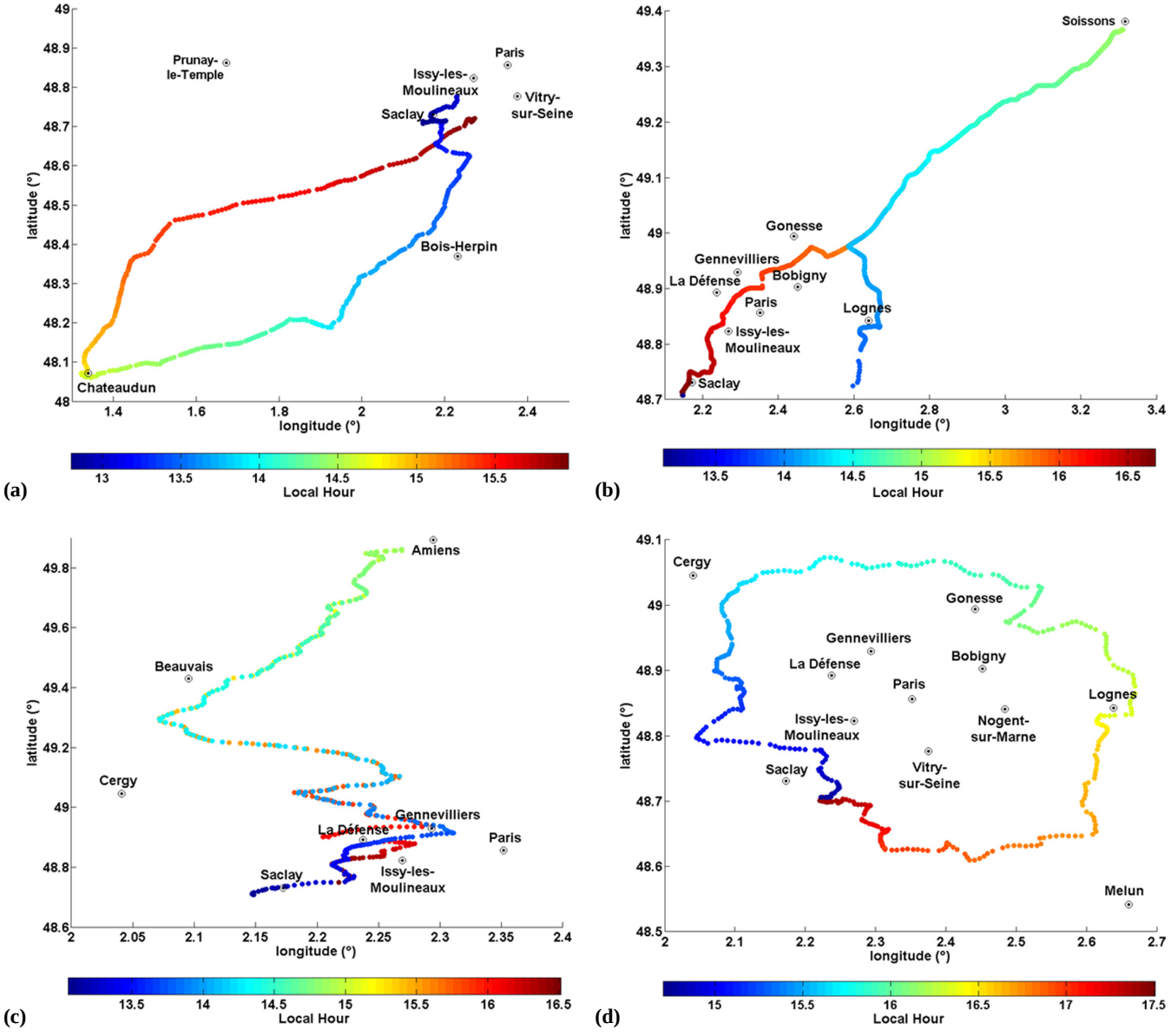

Fig. 2. Lidar van-circuits performed during the MEGAPOLI summer experiment for the 1 **(a)**, 15 **(b)**, 16 **(c)** and 26 **(d)** July 2009. The color scale indicates the decimal hours in LT.

(see yellow triangles on Fig. 1) which were available during MEGAPOLI campaign.

2.2 Lidar-van travelling patterns

2.2.1 Description and rationale

During the MEGAPOLI summer campaign GBML was used to perform measurements along and across the pollution plume emitted by Paris and its suburbs. The main goal was to determine the atmospheric structures (PBL height, cloud and aerosol layers) and the evolution of the aerosol optical properties (aerosol extinction coefficient and depolarization ratio) during its transport from the agglomeration to about 100 km downwind. Aerosol optical properties are indeed functions of the aging and hygroscopic processes acting on pollution particles (Randriamiarisoa et al., 2006). The lidar measurements were triggered based on chemical forecasts delivered by the PREV'AIR system (Rouil et al., 2009; Honoré et al., 2008; www.prevair.org), and which were especially processed for the campaign, for days when the occurrence of a pollution plume downwind of Paris could be expected (light winds in general below about 5 m s^{-1} at 500 m height, cloud free or partially cloudy conditions). Examples of lidar-van circuits are shown in decimal hours (Local Time LT) on Fig. 2 for 1 (2a), 15 (2b), 16 (2c) and 26 July 2009 (2d), for the main representative cases. GBML measurements were

Table 2. Meteorological conditions (wind direction and velocity at ∼250 m, relative humidity at ∼0.2 km and 1 km, levels of pollution (and PM_{10} concentrations), mean AOD (and variability) at 355 nm, mean LR (and variability) and mass increase coefficient u (and variability) during the 10 MD involving GBML during the MEGAPOLI summer experiment.

Day	Hour hh:mm (LT)	Meteorological conditions				Ground-based levels of pollution from AIRPARIF (PM_{10})	AOD ± variability	LR ± variability (sr)	u ± variability
		Wind direction	Wind speed ($m\,s^{-1}$) at ∼250 m	Relative humidity (%)					
				0.2 km	1 km				
01	from 12:48 to 15:58	Northeast	3.3–3.6	51 ± 4	66 ± 3	High (40–90 $\mu g\,m^{-3}$)	0.49 ± 0.14	52.1 ± 6.4	0.23 ± 0.01
02	from 13:01 to 16:00	East	1.0–2.3	49 ± 3	70 ± 3	High (30–70 $\mu g\,m^{-3}$)	0.68 ± 0.06	63.3 ± 14.1	0.21 ± 0.01
04	from 16:49 to 19:24	West	0.9–1.7	50 ± 1	74 ± 2	Low (10–30 $\mu g\,m^{-3}$)	0.22 ± 0.02	80.1 ± 12.6	0.14 ± 0.02
15	from 13:07 to 16:42	Southwest	7.7–8.7	49 ± 2	72 ± 2	low–moderate (20–40 $\mu g\,m^{-3}$)	–	–	0.06 ± 0.01
16	from 13:03 to 16:31	South	3.7–5	47 ± 2	70 ± 3	low-moderate (25–35 $\mu g\,m^{-3}$)	0.23 ± 0.01	29.7 ± 1.2	0.13 ± 0.02
20	from 14:27 to 17:59	West	4.4–5.2	52 ± 2	78 ± 2	Low (10–20 $\mu g\,m^{-3}$)	0.20 ± 0.01	40.7 ± 2.4	0.11 ± 0.01
21	from 13:40 to 16:43	Southwest	8.2–9.8	45 ± 3	63 ± 4	low–moderate (20–40 $\mu g\,m^{-3}$)	–	–	0.15 ± 0.01
26	from 14:42 to 17:30	South	3.5–4.4	45 ± 1	66 ± 1	low (10–20 $\mu g\,m^{-3}$)	0.14 ± 0.01	42.8 ± 8	0.06 ± 0.02
28	from 15:05 to 19:17	Southwest	3.5–4.2	49 ± 2	73 ± 2	low (10–30 $\mu g\,m^{-3}$)	0.18 ± 0.01	34.4 ± 2.1	0.10 ± 0.02
29	from 14:22 to 19:02	Southwest	5.5–7.1	42 ± 1	60 ± 1	low–moderate (20–40 $\mu g\,m^{-3}$)	–	–	0.13 ± 0.02

performed either following the pollution plume (1, 15, 16 20, 21, 28 and 29 July 2009) or by circling in the suburbs of Paris at ∼25 km distance from downtown (for 2, 4 or 26 July 2009). The circular tracks were performed when the meteorological forecasts gave horizontal wind fields not suited for a well-defined pollution plume formation, mainly in the case of an horizontal wind with a mean velocity lower than 4–5 $m\,s^{-1}$.

2.2.2 Meteorological condition and representativity of the spatiotemporal sampling

Table 2 summarizes meteorological conditions (wind direction and speed, relative humidity RH), levels of pollution, AOD, extinction-to-backscatter values (so-called Lidar Ratio LR) at 355 nm and mass increase coefficient u for the 10 measurements days (MD) involving GBML under cloud-free conditions. Wind directions and velocity at ∼250 m and RH are obtained from the Mesoscale Model MM5 and pollution levels from AIRPARIF urban background stations. AOD (± its day-to-day variability) at 355 nm is computed with AOD at 380 nm from Palaiseau AERONET sun-photometer station using the Angström exponent (Angström, 1964) between 340 and 440 nm. Integrated LR values (± its day-to-day variability) are retrieved from coupling between fixed lidar and sun-photometer coincident measurements (see Sect. 4.1). Mass increase coefficients (± its variability in the PBL along the track) have been computed with ISORROPIA thermodynamic model (Nenes et al., 1998).

Table 3. Comparison of air mass origin determined from backward trajectories in the month of July between 2005 and 2010, observed in July 2009 and observed in July 2009 for MD only.

Origin of air masses	July 2005–2010	July 2009	July 2009 (MD only)
Northeast	7 %	3 %	10 %
East	9 %	3 %	10 %
Southeast	3 %	2 %	0 %
South	4 %	5 %	20 %
Southwest	20 %	21 %	40 %
West	41 %	60 %	20 %
Northwest	12 %	6 %	0 %
North	4 %	0 %	0 %

The representativeness of air mass origin observed during the MEGAPOLI summer campaign has been evaluated by comparing with 3-day HYSPLIT (HYbrid Single Particle Lagrangian Integrated Trajectory Model) backward trajectories (http://ready.arl.noaa.gov/HYSPLIT.php) ending at 500 m above ground level (a.g.l.) for the month of July between 2005 and 2010 (Table 3) using as imput $1° \times 1°$ winds from the Global Data Assimilation System (GDAS). The origin of air masses for July 2009 is in good agreement

with the mean of 2005–2010 where most of the air masses came from south-western (20 % for 2005–2010 and 21 % for July 2009) and western sectors (41 % for 2005–2010 and 60 % for July 2009). If we now consider only MD in July 2009 the distribution is significantly different with most air masses observed from the south-western sector (40 %) and an important contribution of the southern sector (20 %) whereas the western sector only represents 20 %. In fact, MD have only been realized in partially cloudy or cloud free conditions, which can explain that the southern sector is over represented and the western sector under represented.

3 Modeling approach

Two Chemistry-transport models (CTM) have been applied to simulate PM_{10} on each MD previously presented. The main characteristics of the two CTMs used in the simulations are summarized in Table 4.

3.1 POLYPHEMUS platform

The POLYPHEMUS air-quality modeling plateform (http://cerea.enpc.fr/polyphemus) is used with the CTM model Polair3D, the gaseous chemistry scheme Regional Atmospheric Chemistry Model (RACM, Stockwell et al., 1997), and the aerosol model SIREAM-AEC (Kim et al., 2011a; Debry et al., 2007; Pun et al., 2002). Polyphemus/Polair3D has already been used for many applications at the continental scale (Sartelet et al., 2007a, 2008; Roustan et al., 2010; Kim et al., 2011b), at the urban/regional scale (Tombette and Sportisse, 2007; Sartelet et al., 2007b; Tombette et al., 2008; Roustan et al., 2011). Three nested simulations are performed here: Europe, France and Greater Paris. The horizontal domain is (35–70° N; 15° W–35° E) with a resolution of $0.5° \times 0.5°$ over Europe, (41–52° N; 5° W–10° E) with a resolution of $0.1° \times 0.1°$ over France and (47.9–50.1° N; 1.2° W–3.5° E) with a resolution of $0.02° \times 0.02°$ over Greater Paris. Over Europe, the horizontal resolution is the same as in Sartelet et al. (2007a), while it is finer than in Tombette and Sportisse (2007) over Greater Paris: 0.02° against 0.05°. Results of the simulation over Paris are used for the comparison to lidar data. In all simulations, 9 vertical levels are considered from the ground to 12 km: 0 m, 40 m, 120 m, 300 m, 800 m, 1500 m, 2400 m, 3500 m, 6000 m and 12 000 m. Concerning the land use coverage, the Global Land Cover Facility (GLCF2000) map with 23 categories is used. The meteorological data are obtained from the 5th Penn State MM5 model (Dudhia, 1993), version 3.6, with a horizontal resolution of 36 km and 25 levels from the ground to 100 hPa height. Biogenic emissions are computed as in Simpson et al. (1999). Over Europe and France, the European Monitoring and Evaluation Program (EMEP, http://www.emep.int/) expert inventory for 2005 is used. Over Greater Paris, anthropogenic emissions are generated with the AIRPARIF inventory for 2000 where available and with the EMEP expert inventory for 2005 elsewhere. More details on the model description and on the use of AIRPARIF and EMEP inventories may be found in Sartelet et al. (2007a) and Tombette and Sportisse (2007) respectively. Further details on the options used in the modeling are given in Table 4.

3.2 CHIMERE model

The second model used here is the eulerian regional chemistry-transport model CHIMERE in its version V2008B (see http://www.lmd.polytechnique.fr/chimere/ for a detailed documentation). The model has been largely applied for continental scale air quality forecast (Honoré et al., 2008; http://www.prevair.org), for sensitivity studies, for example with respect to chemical regimes (Beekmann and Vautard, 2010), and for inverse emission modeling (Konovalov et al., 2006). The model has also been extensively used to simulate photooxidant pollution build-up over the Paris region (e.g. Vautard et al., 2001; Beekmann et al., 2003; Derognat et al., 2003; Deguillaume et al., 2007, 2008), and on several occasions to simulate particulate matter levels over the region (e.g. Bessagnet et al., 2005; Hodzic et al., 2005; Sciare et al., 2010). The initial gas phase chemistry only model has been described by Schmidt et al. (2001) and Vautard et al. (2001), the aerosol modules by Bessagnet et al. (2004, 2008).

The aerosol module includes primary organic (POA) and black carbon (BC), other unspecified primary anthropogenic particulate matter (PM) emissions, wind-blown dust, sea salt, secondary inorganics (sulfate, nitrate and ammonium) as well as secondary organic aerosols (SOA) from anthropogenic and biogenic origin, and particulate water. A sectional size distribution over 8 size bins, geometrically spaced from 40 nm to 10 µm in physical diameter, is chosen. The thermodynamic partitioning of the inorganic mixture (i.e. sulfate, nitrate, and ammonium) is computed using the ISORROPIA model (Nenes et al., 1998, http://nenes.eas.gatech.edu/ISORROPIA), which predicts also the water content. SOA formation of anthropogenic and biogenic origin is predicted by the Pun et al. (2006) scheme, with adaptations described in Bessagnet et al. (2008). The dynamical processes influencing aerosol growth such as nucleation, coagulation and absorption of semi-volatile species are included in the model as described in Bessagnet et al. (2004). In this work, the model is set up on two nested grids: a continental domain (35–57.5° N; 10.5° W–22.5° E) with 0.5° resolution, and a more refined urban/regional domain covering the Ile-de-France and neighboring regions (47.45–50.66° N; 0.35° W–4.41° E) with approximately a 3 km horizontal resolution. Vertical level heights in CHIMERE simulations are: 40 m, 120 m, 240 m, 460 m, 850 m, 1500 m, 2800 m, 5500 m. In both models, density of vertical levels is much enhanced in the first km of the atmosphere. Meteorological input is provided by Penn State University

Table 4. Main characteristics of POLYPHEMUS platform and CHIMERE model.

	POLYPHEMUS	CHIMERE
Number of vertical levels	9 levels from ground to 12 000 m: 0, 40, 120, 300, 800, 1500, 2400, 3500, 6000, 12 000.	8 levels up to 5500 m: 40, 120, 250, 480, 850, 1600, 2900, 5500.
Nestings /horizontal resolution	– Europe (35–70° N; 15° W–35° E) with $0.5° \times 0.5°$ resolution – France (41–52° N; 5° W–10° E) with $0.1° \times 0.1°$ resolution – Ile de France (47.9–50.1° N; 1.2° W–3.5° E) with $0.02° \times 0.02°$ resolution	– continental domain (35–57.5° N; 10.5° W–22.5° E) with $0.5° \times 0.5°$ resolution – regional domain (47.45–50.66° N; 0.35° W–4.41° E) with 3 km resolution
Boundary conditions	Gas: Mozart (climatology) Particles: GOCART (2001)	Gas and particles: LMDz (climatology) LMDZ INCA
Meteorological data	MM5 with a horizontal resolution of 36 km and 25 vertical levels	GFS-MM5 with two nested grids at 45 km (European domain) and 15 km (North-West Europe) horizontal resolution forced by FNL final analysis data from NCAR
Emission inventories	Anthropogenic emissions: Airparif (www.airparif.fr) and EMEP (www.emep.int) where Airparif is not available. Biogenic emissions: as in Simpson et al. (1999)	Anthropogenic emissions: Airparif 2005 (for gases in IdF) EMEP where Airparif is not available. BC and OC from Laboratoire d'Aérologie (Junker and Liousse, 2008) MEGAN for biogenic emission
Emission height of volumic sources	EMEP: Height varying profil which depends on snap categories AIRPARIF: Volumic source emission height given by the inventory	EMEP: Height varying profil which depends on snap categories AIRPARIF: Volumic source emission height given by the inventory
Inorganic parametrization	ISORROPIA (Nenes et al., 1998), bulk equilibrium assumption between gas and particles	ISORROPIA (Nenes et al., 1998)
SOA formation	Mechanistic representation (SuperSorgam, Kim et al., 2011a, b)	Pun et al. (2006); Bessagnet et al. (2008)
Aqueous phase of PM	VSRM (Fahey and Pandis, 2001)	Seinfeld and Pandis (1997)
Computation of liquid water content	ISORROPIA	ISORROPIA
Gaseous chemistry	RACM (Stockwell et al., 1997)	Melchior2
Heterogeneous reactions between gas and aerosol phases	Jacob (2000) with low values for probabilities	Jacob (2000) De Moore et al. (1994) Aumont et al. (2003)
Coagulation of particles	Yes	Yes
Size distribution of PM	5 sections between 0.01 µm and 10 µm	8 sections between 0.01 µm and 10 µm
Parameterization of the vertical diffusion coefficient	Troen and Mahrt (1986)	Troen and Mahrt (1986)

(PSU) National Center for Atmospheric Research (NCAR) MM5 model (Dudhia, 1993) which is run here with two nested grids covering the European domain with a 45 km horizontal resolution and North-Western Europe with a 15 km resolution. MM5 is forced by the National Centers for Environmental Prediction (NCEP) Global Forecast

System (GFS) final (FNL) data. Anthropogenic gaseous and particulate emissions are derived from EMEP annual totals (http://www.ceip.at/emission-data-webdab/). For the nested Ile-de-France grid, refined emissions are used as in Sciare et al. (2010), elaborated by the 6 partners of the EtudeS Multi RégionALes De l'Atmosphère (ESMERALDA) project (AIRPARIF, AIR NORMAND, ATMO PICARDIE, ATMO CHAMPAGNE-ARDENNE, ATMO NORD PAS-DE-CALAIS and LIG'AIR). Biogenic emissions are calculated from the Model of Emissions of Gases and Aerosols from Nature (MEGAN) data base (Guenther et al., 2006). LMDz-INCA (Laboratoire de Météorologie Dynamique zoom – INteractions avec la Chimie et les Aérosols) monthly mean concentrations are used as boundary conditions for gases and aerosols (Hauglustaine et al., 2004).

4 Lidar-derived PM_{10} concentrations

4.1 Aerosol extinction coefficient derived from GBML measurements

The first step before the assessment of the aerosol mass concentration is to derive the aerosol extinction coefficient from the lidar profiles. Fixed ALS450 Rayleigh-Mie lidar profiles from SIRTA (Site Instrumental de Recherche par Télédétection Atmosphérique) have been averaged over 5 min around each sun-photometer measurement. The height-independent LR values (Table 2) are determined using a Klett algorithm (Klett, 1985) to invert the mean lidar profile and a dichotomous approach on LR values converging until the difference between lidar and AERONET sun-photometer AOD at 355 nm is below 10^{-6} (Chazette, 2003). Note that in most of the MD the PBL was well-mixed so that the assumption of a constant lidar ratio throughout the PBL does not lead to a bias in the retrieval of the aerosol extinction coefficient profile. The mean day-to-day values (with their variability) are reported on Table 2. The mean LR during the campaign is ∼49 sr with a high variability of ∼18 sr. On 1, 2 and 16 July 2009, an additional N_2-Raman lidar (NRL) was operational and LR has been derived within the mixed layer independently of the sunphotometer measurements as in Royer et al. (2011). Values of 54.4, 56.1 and 34.9 sr have been retrieved for those three days, respectively. The NRL-derived mean LR is in good agreement with that retrieved from the synergy between GBML and sunphotometer with a discrepancy of ∼5 sr.

The range-corrected backscatter signals from the 10 MD involving the mobile lidar have been inverted into extinction coefficient profiles using a Klett algorithm (Klett, 1985) with the mean integrated LR values determined as described above (see values in Table 2). On 15, 21 and 29 July 2009, when cloudy conditions prevented from retrieving LR values using the sunphotometers, a LR of 34.4 sr has been used corresponding to the value of 28 July 2009 obtained with southwest wind direction. The sources of uncertainty linked to the conversion of lidar measurements in extinction coefficient profiles are discussed in Sect. 4.3.

4.2 Method and optical-to-mass relationships

The method to retrieve PM_{10} concentrations from lidar measurements has been first applied to aerosol observed in an underground railway station of Paris (Raut et al., 2009a, b). The theoretical relationship between PM_{10} and aerosol extinction coefficient ($\alpha_{ext,355}$) is given as a function of the density of particles ρ, the mean cubic radius $\overline{r^3}$ and the mean extinction cross-section $\overline{\sigma_{ext,355}}$ by (Raut and Chazette, 2009):

$$PM_{10}=\rho\cdot\frac{4}{3}\pi\cdot\frac{\overline{r^3}}{\overline{\sigma_{ext,355}}}\cdot\alpha_{ext,355} \quad (1)$$

If we only consider a monomodal lognormal accumulation mode which is sensitive to humidity effect, the cubic modal radius can be written as a function of the modal radius radius r_m and geometrical dispersion of the monomodal distribution σ:

$$\overline{r^3}=r_m^3\cdot\exp\left(\frac{9}{2}\ln^2(\sigma)\right) \quad (2)$$

As the geometrical dispersion is not affected by humidity, we can write Eq. (1) under the following form:

$$PM_{10,wet}=PM_{10,dry}\cdot\underbrace{\frac{\rho_{wet}}{\rho_{dry}}}_{f_u(RH)}\cdot\underbrace{\left(\frac{r_{m,wet}}{r_{m,dry}}\right)^3}_{f_\varepsilon(RH)}\cdot\underbrace{\frac{\sigma_{ext,355,dry}}{\sigma_{ext,355,wet}}}_{1/f_\gamma(RH)}\cdot\frac{\alpha_{ext,355,wet}}{\alpha_{ext,355,dry}} \quad (3)$$

f_u is the aerosol mass growth factor given by (Hänel, 1976):

$$f_u(RH)=\frac{g_u(\max(RH,RH_{ref}))}{g_u(RH_{ref})} \quad (4)$$

$$\text{with}\quad g_u(x)=\frac{1+u\cdot\frac{x}{1-x}}{1+\frac{\rho}{\rho_{H_2O}}\cdot u\cdot\frac{x}{1-x}}$$

where u is the aerosol mass increase coefficient, ρ and ρ_{H_2O} the density of dry particle ($1.7\,g\,cm^{-3}$) and water vapor ($1\,g\,cm^{-3}$) and RH_{ref} the reference RH value which as been taken to 55 % (Randriamiarisoa et al., 2006). The mean day-to-day values of u computed with ISOROPIA in the PBL (and the variability along the track) are reported in Table 2. Note that for 1 and 2 July 2009 with continental air masses advected from Northeast and East, the u values ($u=0.23$ and $u=0.21$, respectively) are close to that found by Randriamiarisoa et al. (2006) ($u=0.23$) under similar conditions.

f_ε is the aerosol size growth factor (Hänel, 1976):

$$f_\varepsilon(RH)=\left(\frac{1-\max(RH,RH_{ref})}{1-RH_{ref}}\right)^{-\varepsilon} \quad (5)$$

Table 5. Slope of the regression analysis (C_0), single scattering albedo ($\omega_{0,355}$) and Angström exponent (a) values used for the calculation of the specific extinction cross-section at 355 nm ($s_{ext,355}$) for urban, peri-urban and rural aerosol types. The uncertainties on the specific extinction cross-sections are also indicated.

Aerosol type	C_0 ($g\,m^{-2}$)	$\omega_{0,355}$	a	$s_{ext,355}$ ($m^2\,g^{-1}$)	Uncertainty on $s_{ext,355}$
Urban	0.981	0.89	2.07	4.5	12 %
Peri-urban	0.821	0.93	2.15	5.9	12 %
Rural	0.386	0.91	1.36	7.1	26 %
Dust	–	0.94	∼0.8	1.1	26 %

with ε the Hänel size growth coefficient. ε and u are linked by the following relationship:

$$\left(\frac{1-\max(\mathrm{RH},\mathrm{RH_{ref}})}{1-\mathrm{RH_{ref}}}\right)^{-\varepsilon}=\left(\frac{1+\frac{\rho}{\rho_{H_2O}}\cdot u\cdot\frac{\max(\mathrm{RH},\mathrm{RH_{ref}})}{1-\max(\mathrm{RH},\mathrm{RH_{ref}})}}{1+\frac{\rho}{\rho_{H_2O}}\cdot u\cdot\frac{\mathrm{RH_{ref}}}{1-\mathrm{RH_{ref}}}}\right)^{1/3} \quad (6)$$

f_γ is the aerosol scattering growth factor (Hänel, 1976):

$$f_\gamma(\mathrm{RH})=\left(\frac{1-\max(\mathrm{RH},\mathrm{RH_{ref}})}{1-\mathrm{RH_{ref}}}\right)^{-\gamma} \quad (7)$$

with γ the Hänel scattering growth coefficient. Randriamiarisoa et al. (2006) reported values of γ between 1.04 and 1.35 in a suburban area south of Paris. In this study we used a mean value of 1.2 ± 0.15.

An empirical optical-to-mass relationship between $PM_{10,dry}$ concentrations in PBL and dry extinction coefficient $\alpha_{ext,355,dry}$ has been established from nephelometer and TEOM in-situ measurements (Raut and Chazette, 2009):

$$\mathrm{PM_{10,dry}}=\underbrace{C_0\cdot\omega_{0,355}\cdot\left(\frac{700}{355}\right)^{-a}}_{1/s_{ext,355}}\alpha_{ext,355,dry} \quad (8)$$

where $s_{ext,355}$ is the specific extinction cross-section at 355 nm, $\omega_{0,355}$ is the single-scattering albedo at 355 nm and a the Angström exponent between 450 and 700 nm which is assumed to be the same as the Angström exponent between 355 and 700 nm. C_0 is the slope of regression analysis between the nephelometer scattering coefficients at 700 nm and the TEOM PM_{10} measurements performed simultaneously during several campaigns in Paris and its suburbs.

By combining Eqs. (3) and (8) we can derive a wet PM_{10} concentration with $\alpha_{ext,355,wet}$ measured from lidar:

$$\mathrm{PM_{10,wet}}=C_0\cdot\omega_{0,355}\cdot\left(\frac{700}{355}\right)^{-a}\cdot\frac{f_u(\mathrm{RH})\cdot f_\varepsilon(\mathrm{RH})^3}{f_\gamma(\mathrm{RH})}\cdot\alpha_{ext,\,355,wet} \quad (9)$$

Raut and Chazette (2009) have determined different values of C_0, $\omega_{0,355}$, a and $s_{ext,355}$ for dust, urban, peri-urban, rural aerosol types (see Table 5). A relationship for urban type aerosol has been determined from in-situ measurements in the center of Paris during ESQUIF (Chazette et al., 2005) and LISAIR (Raut and Chazette, 2007) campaigns, respectively in 1999 and 2005. Peri-urban situations have been identified during ParisFog in 2007 (Elias et al., 2009) and during ESQUIF in 1999. They correspond to measurements directly influenced by urban sources, but taken outside urban centers. Rural conditions influenced by pollution in the Paris area have been encountered during the MEAUVE campaign in 2001 (Lavigne et al., 2005). Concerning dust aerosols it has not been possible to determine statistical relationships due to the lack of dust events reaching the surface at Paris. A dust specific cross-section has been determined using a theoretical relationship given in Eq. (1) (Raut and Chazette, 2009) assuming a mean density ($2\,g\,cm^{-3}$), a mean cubic radius ($7.03\times10^{-3}\,\mu m^3$) and a mean extinction cross-section ($6.72\times10^{-10}\,cm^2$). For the comparisons with AIRPARIF and CTMs simulations, the urban parametrization will be used for lidar observations inside the pollution plume in the inner suburbs of Paris, the peri-urban relationship for measurements outside the pollution plume in the inner suburbs and measurements inside the plume far from Paris. A rural relationship will be applied for observations far from Paris center outside the pollution plume. A combination of dust and pollution aerosol specific extinction cross-sections is used on 15 July 2009 where a mixing of dust and pollution aerosols is observed. The different sources of uncertainties on the retrieval of PM_{10} from lidar measurements are discussed in the following section.

4.3 Uncertainties on PM_{10}

The retrieval of PM_{10} from lidar measurements is affected by uncertainties: on the determination of extinction coefficient profiles, on the specific extinction cross-sections at 355 nm, on the assumption linked to the aerosol type (urban, peri-urban, rural or dust), and on hygroscopic effect on aerosols due to RH.

Lidar measurements are inverted into extinction coefficient profiles using a Klett algorithm with the mean LR value in Table 2. Considering an uncertainty of 0.02 (Holben et al., 1998) on the AOD sun-photometer constraint, the total relative uncertainty on the extinction coefficient profile is 21 %, 13 % and 8 % for a mean AOD of 0.1, 0.2 and 0.5 at 355 nm, respectively (Royer et al., 2011). These calculations take into account (1) the uncertainty on the a priori knowledge of the vertical profile of the molecular backscatter coefficient as determined from ancillary data, (2) the uncertainty of the lidar signal in the altitude range used for the normalization, (3) the statistical fluctuations in the measured signal, associated with random detection processes and (4) the uncertainty on the AOD sun-photometer constraint. One has also to consider

the uncertainty in the extinction coefficient due to the evolution of LR values along the track. To assess this uncertainty we have considered the day-to-day variability of the LR retrieved from fixed lidar measurements which is comprised between 4 % and 23 %. An uncertainty of 5 %, 10 %, 15 %, 20 % and 25 % leads to an uncertainty of 2.5 %, 5.5 %, 9 %, 11 % and 14 % on extinction coefficient profiles.

Uncertainties in the specific extinction cross-sections have been assessed as 12 % (resp. 26 %) for urban and peri-urban (resp. dust and rural) relationships taking into account uncertainties on C_0, $\omega_{0,355}$ and a (Raut and Chazette, 2009).

Only uncertainties linked to the measurements are quantified here. Concerning the aerosol type assumption, uncertainties are linked to the empirical optical-to-mass relationship, which assumes a particular chemical composition and granulometry for each aerosol type. Taking a peri-urban relationship instead of an urban (resp. rural) relationship leads to an underestimation (resp. overestimation) of PM_{10} concentration of 30 % (resp. 20 %).

The influence of hygroscopicity has been neglected for the comparisons with AIRPARIF dry $PM_{10,dry}$ (Sect. 4.4) since RH values observed (see Table 2) during the 10 MD stay below 55 % at 200 m height. The liquid water content of particles computed from ISOROPIA (Nenes et al., 1998) using the particulate composition of POLYPHEMUS (see Sect. 4) along the lidar trajectories indicates that water represents in average 25.5 % on 1 July, 20.4 % on 2 July, 14.4 % on 4 July, 6.7 % on 15 July, 12.7 % on 16 July, 12.3 % on 20 July, 12.7 % on 21 July, 5.4 % on 26 July, 11.3 % on 28 July and 10.0 % on 29 July of dry modeled PM_{10} concentrations. For the comparisons of wet integrated PM_{10}, the uncertainty on RH has been assessed to 11 % in the PBL by comparison between MM5 and Trappes radiosoundings, the uncertainty on u has been evaluated with the day-to-day variability of u along the track and the uncertainty on γ has been taken to 0.15. The uncertainty on each parameter has been assessed with a Monte Carlo approach by varying one parameter after the other and keeping the other constant. The different sources of uncertainty are supposed to be independent so that the uncertainty on hygroscopic effect is computed by taking the square root of the quadratic sum of each source of uncertainty.

The expected uncertainties on PM_{10} at 200 m (Table 6) and wet integrated PM_{10} (Table 7) have been computed for each MD considering the mean AOD, the variability of LR, the uncertainty on γ and u, the uncertainty on the specific extinction cross-section and on RH values. For PM_{10} concentrations at 200 m the uncertainty ranges from 16 to 23 % (resp. 28 to 33 %) with a mean value of 19 % (resp. 30 %) for peri-urban and urban (resp. rural and dust) relationships. The uncertainty on the specific extinction cross-section, on lidar/sun-photometer coupling and on the evolution of LR along the track represent 44 % (resp. 77 %), 40 % (resp. 16 %) and 16 % (resp. 7 %) of total uncertainty for peri-urban and urban (resp. rural and dust) relationships, respectively. The mean expected uncertainty on lidar integrated PM_{10} is 21 % with peri-urban and urban and 31 % with rural and dust relationships. With peri-urban and urban relationships, the uncertainties on the specific extinction cross-section, on the hygroscopic effect, on lidar/sun-photometer coupling, and on the evolution of LR along the track account for 36 %, 17 %, 34 % and 13 % of total uncertainty. With rural and dust relationships the corresponding values are 71 %, 8 %, 15 % and 6 %, respectively.

4.4 Comparison between GBML-derived PM_{10} and AIRPARIF measurements

Figures 3 and 5 show the spatial distributions of wet PM_{10} at ∼250 m a.g.l. (where the lidar overlap function reaches 1) on 1 (3a), 15 (3b), 16 (5a) and 26 (5b) July 2009. Lidar-derived and AIRPARIF ground-based PM_{10} are shown in the left column. Winds at ∼250 m a.g.l. used in POLYPHEMUS and CHIMERE simulations are also indicated with black arrows to highlight the direction of the pollution plume for each model.

Comparisons between lidar and AIRPARIF PM_{10} have been expressed for each relationship (urban, peri-urban and rural) in terms of Root Mean Square Error (RMSE) and Mean Absolute Percentage Error (MAPE) given by the following equations:

$$\mathrm{RMSE} = \sqrt{\frac{1}{n}\sum_{i=1}^{n}(\mathrm{PM_{10}}^{\mathrm{mod}} - \mathrm{PM_{10}^{mes}})^2} \quad (10)$$

$$\mathrm{MAPE} = \frac{100}{n}\sum_{i=1}^{n}\frac{\left|\mathrm{PM_{10}}^{\mathrm{mod}} - \mathrm{PM_{10}^{mes}}\right|}{\left(\frac{\mathrm{PM_{10}}^{\mathrm{mod}} + \mathrm{PM_{10}^{mes}}}{2}\right)} \quad (11)$$

where n is the number of observations and, $\mathrm{PM_{10}^{mod}}$ and $\mathrm{PM_{10}^{mes}}$ are the modeled and measured PM_{10}, respectively. RMSE and MAPE are both summarized in Table 6. Only AIRPARIF stations located at less than 10 km from GBML are considered for the comparisons. Any corrections of humidity effect at 200 m height, lidar wet PM_{10} have been directly compared with dry PM_{10} concentrations measured by AIRPARIF without any correction of the humidity effect.

The 1 July 2009 (Fig. 3a) is characterized by high surface temperatures (up to 30 °C) and anticyclonic conditions. Lidar measurements are performed leeward inside the pollution plume in the southwest of Paris from Saclay (latitude 48.73° N; longitude 2.17° E) to Chateaudun (latitude 48.1° N; longitude 1.34° E) between 12:48 and 15:58 LT. It is the most polluted day of the campaign with high levels of PM_{10}, on the average $42 \pm 16\,\mu g\,m^{-3}$ obtained with the peri-urban relationship at 210 m height along the GBML van-circuit and between 40 and $80\,\mu g\,m^{-3}$ measured by AIRPARIF background stations. Only peri-urban and rural relationships have to be considered for this MD as measurements have been realized far from the sources inside and

Table 6. Root Mean-Square Errors (RMSE) and Mean Absolute Percentage Error (MAPE) on PM_{10} calculated for each MD between GBML/POLYPHEMUS, GBML/CHIMERE, GBML/AIRPARIF, POLYPHEMUS/AIRPARIF and CHIMERE/AIRPARIF at ground level and ∼250 m height. The comparisons with GBML measurements have been made with rural, peri-urban and urban relationships. The expected uncertainties on GBML-derived PM_{10} have also been computed for rural, peri-urban and urban relationships taking into account AOD observed during each MD. Note that for 15 July a mixing of dust and peri-urban relationships has been used in lidar inversion.

Day	Optical-to-mass relation-ships	Mean wet PM_{10}± variability ($\mu g\,m^{-3}$)			Root Mean Square Error in $\mu g\,m^{-3}$ (and Mean Absolute Percentage Error in %)					Expected uncer-tainty on lidar PM_{10} (%)
					Ground level			∼250 m		
		Lidar	POLY-PHEMUS	CHIMERE	AIRPARIF/Lidar	AIRPARIF/ POLY-PHEMUS	AIRPARIF/ CHIMERE	Lidar/ POLYPHEMUS	Lidar/ CHIMERE	
01	Urban	54.1±20.7	45.5±16.3	32.8±10.0	18.1 (30.4 %)	14.3 (26.6 %)	14.5 (29.5 %)	12.9 (19.3 %)	25.2 (45.7 %)	16 %
	Peri-urban	42.0±16.1			3.2 (5.6 %)			8.2 (13.4 %)	13.2 (24.2 %)	16 %
	Rural	33.9±13.0			8.8 (16.0 %)			13.7 (29.8 %)	7.2 (16.7 %)	28 %
02	Urban	60.2±7.1	32.5±3.6	31.8±4.0	19.6 (38.3 %)	16.4 (42.5 %)	12.5 (26.8 %)	28.9 (60.4 %)	29.1 (61.3 %)	19 %
	Peri-urban	46.8±5.5			7.0 (14.4 %)			15.9 (38.7 %)	15.9 (38.4 %)	19 %
	Rural	37.8±4.4			6.1 (11.6 %)			8.0 (20.0 %)	7.6 (19.5 %)	30 %
04	Urban	24.5±2.1	11.9±2.7	13.9±5.3	6.5 (29.2 %)	7.8 (48.6 %)	7.6 (41.6 %)	12.9 (69.8 %)	11.5 (59.5 %)	19 %
	Peri-urban	19.0±1.6			1.0 (4.7 %)			7.6 (47.1 %)	7.0 (41.5 %)	19 %
	Rural	15.4±1.3			3.1 (17.2 %)			4.3 (29.2 %)	5.1 (27.6 %)	30 %
15	Urban	25.5±2.4	16.5±0.8	18.4±1.1	4.3 (10.5 %)	7.8 (27.8 %)	6.7 (22.2 %)	9.3 (42.6 %)	7.6 (32.0 %)	–
	Peri-urban	22.5±2.1			5.8 (18.3 %)			6.4 (30.7 %)	4.8 (20.3 %)	–
	Rural	20.5±1.9			7.3 (25.4 %)			4.5 (21.8 %)	3.1 (13.2 %)	–
16	Urban	23.6±3.4	22.7±2.2	14.7±2.4	6.9 (26.0 %)	3.3 (11.2 %)	9.6 (29.7 %)	4.0 (13.0 %)	9.8 (46.3 %)	17 %
	Peri-urban	18.4±2.7			10.8 (44.3 %)			5.4 (22.2 %)	5.1 (24.9 %)	17 %
	Rural	14.8±2.2			13.6 (64.0 %)			8.4 (42.1 %)	3.2 (15.7 %)	28 %
20	Urban	16.0±1.6	17.4±2.1	11.6±1.3	2.6 (12.2 %)	1.3 (5.4 %)	4.6 (28.4 %)	2.6 (10.9 %)	4.6 (31.5 %)	18 %
	Peri-urban	12.4±1.2			4.7 (28.4 %)			5.4 (33.2 %)	1.6 (11.0 %)	18 %
	Rural	10.0±1.0			6.9 (48.9 %)			7.6 (53.6 %)	2.0 (16.1 %)	29 %
21	Urban	26.9±3.6	20.7±1.8	20.8±3.5	11.7 (26.5 %)	15.5 (40.1 %)	15.6 (43.2 %)	7.1 (25.9 %)	7.4 (26.2 %)	–
	Peri-urban	20.9±2.8			16.9 (50.5 %)			2.8 (10.8 %)	3.9 (14.9 %)	–
	Rural	16.9±2.3			20.6 (69.8 %)			4.5 (21.9 %)	5.4 (23.5 %)	–
26	Urban	17.1±1.3	8.1±1.1	8.8±1.9	2.6 (15.1 %)	6.6 (51.4 %)	4.5 (35.0 %)	9.0 (71.2 %)	8.4 (65.7 %)	23 %
	Peri-urban	13.3±1.0			1.8 (10.2 %)			5.2 (48.3 %)	4.7 (42.4 %)	23 %
	Rural	10.7±0.8			4.3. (31.2 %)			2.7 (27.9 %)	2.3 (23.6 %)	33 %
28	Urban	16.7±2.0	13.1±2.6	11.2±1.7	6.7 (35.8 %)	5.9 (29.8 %)	5.2 (27.5 %)	4.4 (25.8 %)	6.2 (40.5 %)	19 %
	Peri-urban	13.0±1.5			8.2 (43.7 %)			2.4 (15.8 %)	2.9 (20.1 %)	19 %
	Rural	10.5±1.2			9.8 (55.0 %)			3.5 (23.1 %)	2.2 (15.8 %)	30 %
29	Urban	20.7±2.5	11.3±1.8	11.0±1.6	9.1 (27.7 %)	12.4 (41.9 %)	13.3 (44.2 %)	9.6 (59.4 %)	9.9 (61.9 %)	–
	Peri-urban	16.1±2.0			12.6 (40.4 %)			5.0 (35.7 %)	5.2 (38.4 %)	–
	Rural	13.0±1.6			15.4 (60.1 %)			2.0 (15.5 %)	2.2 (17.4 %)	–
mean	Urban	28.5±4.7	20.0±3.5	17.5±3.3	8.8 (25.2 %)	9.1 (32.5 %)	9.4 (32.8 %)	10.1 (39.8 %)	11.9 (47.1 %)	19 %
	Peri-urban	22.4±3.7			7.2 (26.0 %)			6.4 (29.6 %)	6.4 (27.6 %)	19 %
	Rural	18.4±3.0			9.6 (39.9 %)			5.9 (28.5 %)	4.0 (18.9 %)	30 %

outside the pollution plume. The highest values of GBML-derived PM_{10} (70–90 $\mu g\,m^{-3}$ for peri-urban relationship) are observed at the beginning of the track, in agreement with the values measured at 13h LT by AIRPARIF at Issy-les-Moulineaux (66 $\mu g\,m^{-3}$) and La Défense (78 $\mu g\,m^{-3}$) in the southwest of Paris. The decrease of PM_{10} from the center of Paris to its suburb is clearly visible on both AIRPARIF and GBML profiles. GBML-derived PM_{10} decreases down to 50 $\mu g\,m^{-3}$ with peri-urban relationship near Bois Herpin (47 $\mu g\,m^{-3}$ measured by AIRPARIF at 14:00 LT) and down to 20 $\mu g\,m^{-3}$ near Chateaudun with the rural parametrization. We can notice the lower concentrations observed near Saclay at 16:00 LT than at 13:00 LT (58 compared with 87 $\mu g\,m^{-3}$ with the peri-urban relationship, Fig. 4a and 4c). This is probably explained by the increase of the PBL height from 1.2 up to 1.8 km leading to a dilution of pollutants. Note that the increase observed at the top of the PBL is due to a hygroscopic effect, indeed RH from MM5 model increases up to 70 % at ∼1.2 km and to 70 % at 2km from ATR-42 measurements near Chateaudun at ∼17:00 (LT). A strong thermic convection occurring in the well developed convective mixing layer observed during this day can explain the good

Table 7. Comparisons of wet integrated PM_{10} between the ground level and 1 km a.g.l. from GBML, POLYPHEMUS and CHIMERE.

Day	Optical-to-mass relationships	Mean wet integrated $PM_{10}\pm$ variability in mg m^{-2}			Root Mean Square Error on wet integrated PM_{10} in mg m^{-2} (and Mean Absolute Percentage Error in %)		Expected uncertainty on lidar integrated PM_{10} (%)
		Lidar	POLYPHEMUS	CHIMERE	Lidar/ POLYPHEMUS	Lidar/ CHIMERE	
01	Urban	47.2±21.3	49.7±13.3	28.7±6.0	12.4 (22.4 %)	25.0 (42.4 %)	18 %
	Peri-urban	36.7±16.6			15.5 (36.9 %)	14.6 (27.9 %)	18 %
	Rural	29.6±13.4			21.2 (55.7 %)	9.1 (26.7 %)	30 %
02	Urban	52.0±9.5	37.7±3.7	30.8±4.1	17.9 (37.0 %)	22.9 (52.8 %)	21 %
	Peri-urban	40.4±7.4			9.3 (17.3 %)	11.8 (31.0 %)	21 %
	Rural	32.6±5.9			9.1 (17.4 %)	6.1 (15.8 %)	31 %
04	Urban	18.0±2.9	12.4±2.7	13.2±4.9	6.5 (36.9 %)	6.5 (38.2 %)	22 %
	Peri-urban	14.0±2.2			3.5 (20.1 %)	4.4 (21.8 %)	22 %
	Rural	11.3±1.8			3.1 (19.4 %)	4.8 (23.4 %)	32 %
15	Urban	19.9±2.1	15.9±0.7	16.5±0.8	4.5 (22.1 %)	4.2 (19.2 %)	–
	Peri-urban	17.6±1.9			2.5 (12.1 %)	2.4 (11.4 %)	–
	Rural	16.0±1.7			1.7 (8.3 %)	2.1 (10.5 %)	–
16	Urban	19.1±3.4	22.0±2.0	13.7±1.9	4.7 (19.1 %)	6.7 (33.2 %)	18 %
	Peri-urban	14.8±2.6			7.8 (39.6 %)	3.5 (17.8 %)	18 %
	Rural	12.0±2.1			10.4 (59.5 %)	3.4 (21.1 %)	30 %
20	Urban	11.6±1.3	19.5±3.1	10.9±1.3	8.5 (49.9 %)	1.7 (12.9 %)	22 %
	Peri-urban	9.0±1.0			10.1 (75.3 %)	2.4 (20.0 %)	22 %
	Rural	7.3±0.8			12.6 (90.3 %)	3.9 (39.7 %)	32 %
21	Urban	20.7±3.6	21.2±1.7	19.4±3.3	3.5 (13.7 %)	4.4 (17.9 %)	–
	Peri-urban	16.1±2.8			5.9 (28.9 %)	5.0 (23.0 %)	–
	Rural	13.0±2.2			8.6 (49.0 %)	7.3 (39.7 %)	–
26	Urban	13.2±1.3	8.1±1.2	8.1±1.8	5.2 (48.2 %)	5.2 (49.6 %)	24 %
	Peri-urban	10.3±1.0			2.3 (24.2 %)	2.4 (26.0 %)	24 %
	Rural	8.3±0.8			0.9 (7.2 %)	1.2 (11.0 %)	33 %
28	Urban	12.3±1.9	12.9±2.3	10.5±1.4	2.3 (14.9 %)	2.9 (19.5 %)	19 %
	Peri-urban	9.6±1.5			4.0 (30.2 %)	2.2 (17.1 %)	19 %
	Rural	7.7±1.2			5.6 (49.6 %)	3.3 (31.7 %)	30 %
29	Urban	16.8±2.2	11.2±1.6	10.0±1.5	5.9 (40.9 %)	7.0 (51.1 %)	–
	Peri-urban	13.1±1.7			2.3 (16.8 %)	3.3 (27.1 %)	–
	Rural	10.6±1.4			1.2 (8.2 %)	1.1 (8.6 %)	–
mean	Urban	23.1±5.0	21.1±3.2	16.2±2.7	7.1 (30.5 %)	8.9 (33.7 %)	21 %
	Peri-urban	18.2±3.9			6.3 (30.1 %)	5.2 (22.3 %)	21 %
	Rural	14.8±3.1			7.4 (36.5 %)	4.2 (22.8 %)	31 %

correlation observed between PM_{10} at ground and 210 m levels. For this MD, RMSE (MAPE) between GBML and AIRPARIF data is 3.2 and 8.8 µg m^{-3} (5.6 and 16 %) using peri-urban and rural relationships.

On 15 July 2009, dust aerosol layers were observed by the lidar measurements as confirmed by the Dust Regional Atmospheric Model (DREAM, http://www.bsc.es/projects/earthscience/DREAM) and the low Angström exponent close to 0.5 measured by the Palaiseau AERONET sun-photometer. The increase between 08:00 and 09:00 LT of background PM_{10} and the decrease from 55 % to 35 % of $PM_{2.5}/PM_{10}$ ratio reported by the AIRPARIF network suggest that dust aerosols have been mixed into the PBL and have reached the surface. At the same time the Palaiseau sun-photometer has measured a slight increase of AOD at 355 nm from 0.16 to 0.19. This increase is used to assess the proportion of dust and pollution extinction specific cross-sections at 355 nm. Figures 3b and 6b show the spatial and temporal evolution of PM_{10} at 210 m along the track. For this MD, lidar measurements have mainly been performed under urban and peri-urban conditions. If we only consider pollution aerosols within the PBL, PM_{10} are underestimated compared with AIRPARIF by 10.8 and 14.2 µg m^{-3} (MAPE of 47.3 % and 70.2 %) with the urban and peri-urban parametrizations,

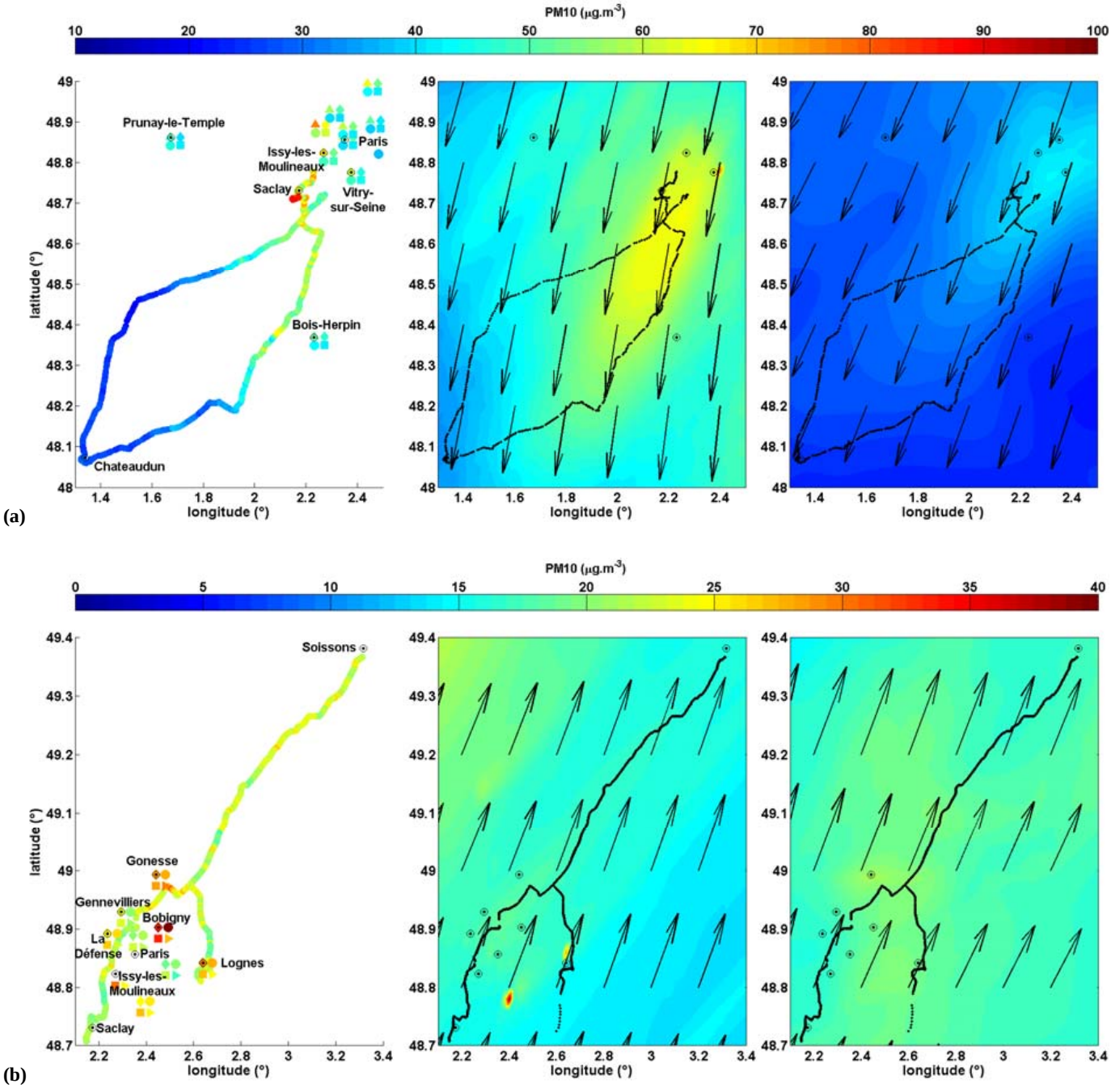

Fig. 3. Spatial distributions of wet PM_{10} at 12:00 (UT) on 1 **(a)** and 15 **(b)** July derived from lidar measurements with the peri-urban relationship at 210 m height (left column) and simulated at 12:00 (UT) with the POLYPHEMUS model at 210 m height (central column) and the CHIMERE model at 250 m height (right column). Black arrows representing the wind at ∼250 m height used in POLYPHEMUS and CHIMERE simulations are shown on the central and right panels. Dry PM_{10} from AIRPARIF ground-based network are indicated by filled symbols at 13:00 (up triangles), 14:00 (diamonds), 15:00 (rounds), 16:00 (squares), 17:00 (right triangles), 18:00 LT (pentagrams) in the left column. Note that for 15 July a mixing of dust and peri-urban relationships has been used in lidar inversion.

respectively. Considering a contribution of 54 % of dust aerosols in the total PM_{10}, no underestimation is observed and the RMSE is 4.3 and 5.8 µg m^{-3} (10.5 and 18.3 %) with urban and peri-urban relationships. Indeed, this better comparison indicates the presence of a mixed aerosol for this day. On that day, the mean PM_{10} observed by GBML is 25.5 ± 2.4 µg m^{-3} (resp. 22.5 ± 2.1 µg m^{-3}) with urban (resp. peri-urban) relationships.

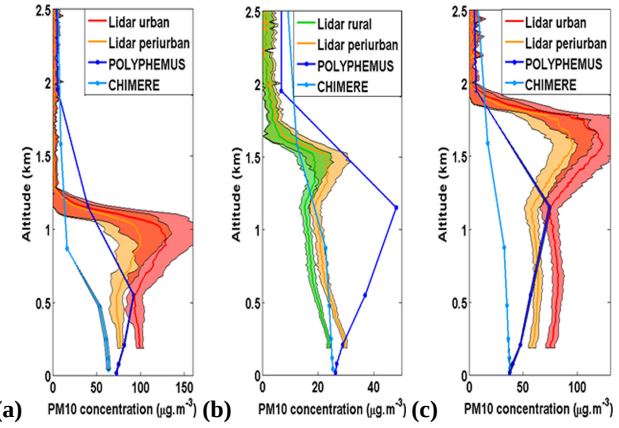

Fig. 4. Vertical profiles of PM_{10} concentrations on 1 July at the beginning of the van track near Saclay **(a)**, at Chateaudun **(b)** and at the end near Saclay **(c)**. Data have been averaged over 20 lidar profiles: the mean profile is represented by the solid line and the variability by the shaded area. Lidar measurements below the altitude of full overlap are not represented in these profiles.

On 16 July 2009 (Fig. 5a) GBML measurements are performed in the north of Paris from Saclay (latitude 48.73° N; longitude 2.17° E) to Amiens (latitude 49.89° N; longitude 2.29° E) between 13:00 to 16:30 LT. According to criteria detailed in Sect. 4.2, the urban relationship is considered for comparison with AIRPARIF stations located inside the pollution plume (La Défense, Issy-les-Moulineaux and Gennevilliers), peri-urban relationship is considered for measurements far from Paris inside the pollution plume (near Beauvais) and rural relationship for measurements outside the pollution plume near Amiens. Moderate levels of pollutions (25–35 $\mu g\,m^{-3}$) are observed at Issy-les-Moulineaux, La Défense and Gennevilliers AIRPARIF stations located in the north and the west of Paris, in agreement with GBML-derived PM_{10} (22–25 $\mu g\,m^{-3}$ for the urban relationship). GBML-derived PM_{10} progressively decreases to reach 10 $\mu g\,m^{-3}$ for the rural relationship near Amiens. Only AIRPARIF urban stations under the pollution plume have been compared with lidar measurements. The RMSE (MAPE) is 6.9 $\mu g\,m^{-3}$ (26 %) with the urban relationship for a mean value of PM_{10} between 18.4 and 23.6 $\mu g\,m^{-3}$ for GBML with a peri-urban and a urban relationship, respectively.

On 26 July 2009 a circular lidar-van travelling pattern was realized from 14:40 to 17:30 LT at a distance between 15 and 30 km from Paris center (Fig. 5b). Urban relationship must be considered in the North-Northeast of Paris inside the pollution plume (for the comparisons with Gonesse AIRPARIF stations) and peri-urban relationship for the other stations. With these criteria RMSE is 1.7 $\mu g\,m^{-3}$ and MAPE is 9.4 %. Low levels of pollution have been observed (GBML-derived PM_{10} mean values between 13.3 and 17.1 $\mu g\,m^{-3}$ with peri-urban and urban parametrizations) with background concentration around 13–14 $\mu g\,m^{-3}$ (La Défense, Issy-les-Moulineaux, Vitry-sur-Seine and Lognes AIRPARIF stations) and a slight increase to 18–20 $\mu g\,m^{-3}$ leeward in the north of Paris (Gonesse and Bobigny AIRPARIF stations).

It is noteworthy that PM_{10} measured at Bobigny and Gonesse AIRPARIF stations is particularly high compared with GBLM retrievals especially for southwest wind directions (15, 21, 28 and 29 July). These stations may be influenced by local emissions from Le Bourget airport located 4–5 km in the southwest of Gonesse and from industrial activities (railway activities) located 0.5–3 km in the southwest of Bobigny. If we exclude these stations, the RMSE between GBML with a peri-urban and AIRPARIF decreases from 5.8 to 3 $\mu g\,m^{-3}$ on 15 July, from 16.9 to 11.0 $\mu g\,m^{-3}$ on 21 July and from 8.2 to 3.7 $\mu g\,m^{-3}$ on 28 July.

Considering the 10 MD with all AIRPARIF stations, the mean total RMSE between GBML-derived PM_{10} and AIRPARIF measurements are 7.2 $\mu g\,m^{-3}$ and 8.8 $\mu g\,m^{-3}$ with peri-urban and urban relationships (where most of the comparisons have been realized) and the mean MAPE are 26 % and 25.2 % for mean values of 22.4 ± 3.7 and 28.5 ± 4.7 $\mu g\,m^{-3}$, respectively (Table 6). If we exclude Bobigny and Gonesse stations, the RMSE (and MAPE) decrease to 5.9 $\mu g\,m^{-3}$ (24.6 %) for GBML with a peri-urban relationship and 7.8 $\mu g\,m^{-3}$ (23.5 %) for GBML with a urban relationship. These discrepancies are in good agreement with the expected uncertainty of 19 % computed for urban and peri-urban relationships (see Table 6). Two additional factors have to be taken into account: (1) uncertainties in PM_{10} measured by TEOM instruments (between 15 and 20 %, see Sect. 2.1.2) and (2) the possible decorrelation between ground level and PM_{10} values at 210 m a.g.l. Note that significant variations in the aerosol optical signature have been previously observed around Paris by Chazette et al. (2005) and Raut and Chazette (2009) within the first hundred meters above the surface. Thus, differences between lidar derived PM_{10} concentrations and AIRPARIF observations are clearly within the range of expected errors.

5 Comparison with chemistry-transport models

CTMs compute concentrations of pollutants at predefined vertical heights. Wet PM_{10} at height levels computed by the CTM have been compared to GBML-derived PM_{10}. At each GBML position and each CTM's vertical height, wet PM_{10} calculated by the CTM are interpolated horizontally and temporally. We present here comparisons at ground and ~200 m a.g.l. The integrated content of PM_{10} derived from both lidar measurements and modeling are also compared to reflect the lidar information within PBL.

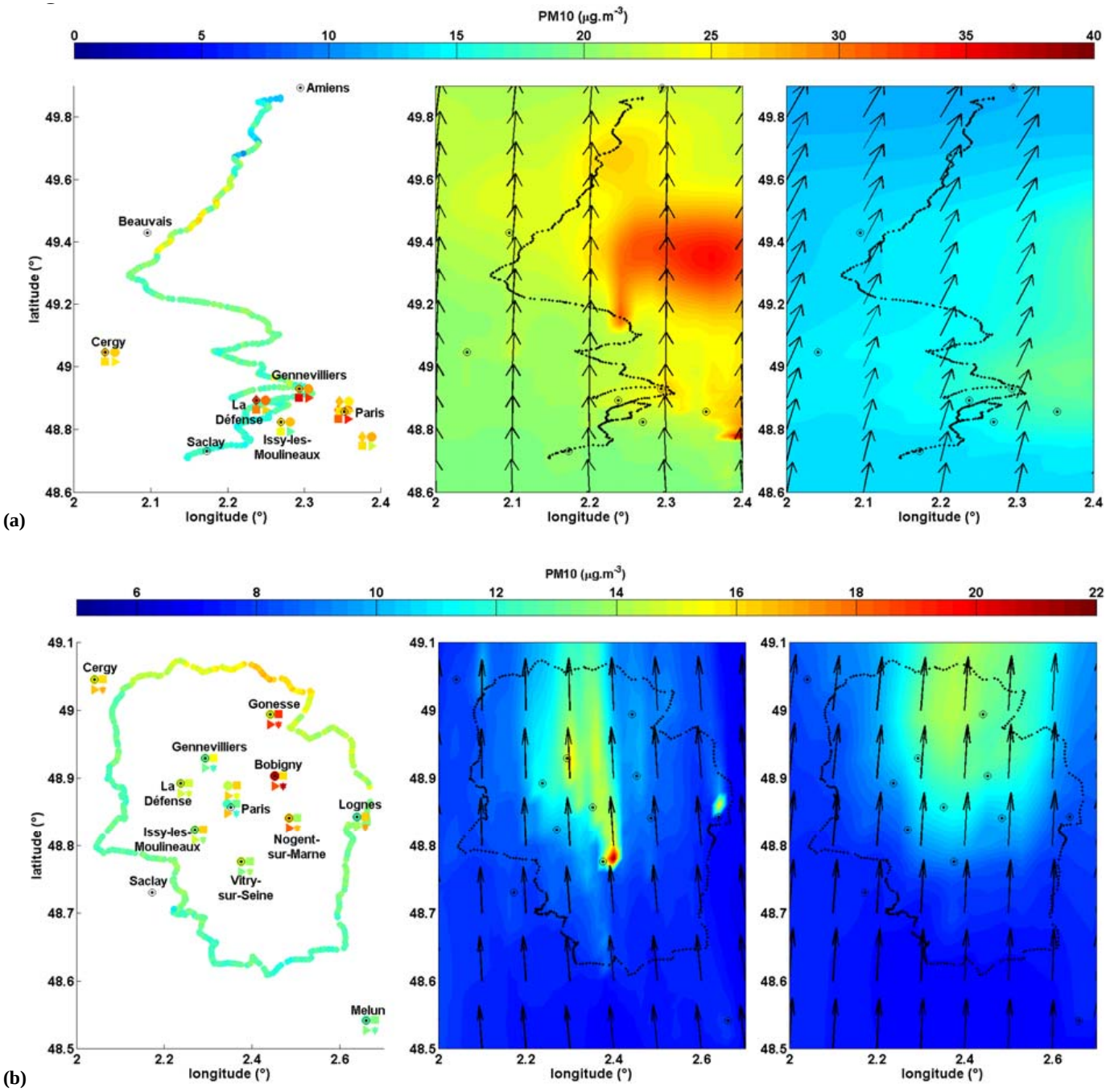

Fig. 5. Same as Fig. 3 on 16 **(a)** and 26 **(b)** July.

5.1 Comparison between lidar and modeling within the low PBL

Figures 3 and 5 show the spatial distribution of wet PM_{10} at ∼200 m a.g.l. modeled by POLYPHEMUS and CHIMERE CTMs (central and right panels, respectively) on 1, 15, 16 and 26 July 2009 at 12:00 (UT). On Fig. 6 lidar wet PM_{10} measurements estimated with rural (green), peri-urban (orange) and urban (red) relationships are compared with wet PM_{10} modeled along the track with POLYPHEMUS (dark blue) and CHIMERE (light blue) CTMs. Dry PM_{10} at the ground level from AIRPARIF and the lowest model layer of POLYPHEMUS and CHIMERE are also indicated by black, dark blue and light blue filled symbols, respectively.

Most of the comparisons between lidar and models have been realized far from Paris inside the pollution plume or close to Paris outside the pollution plume. We thus consider

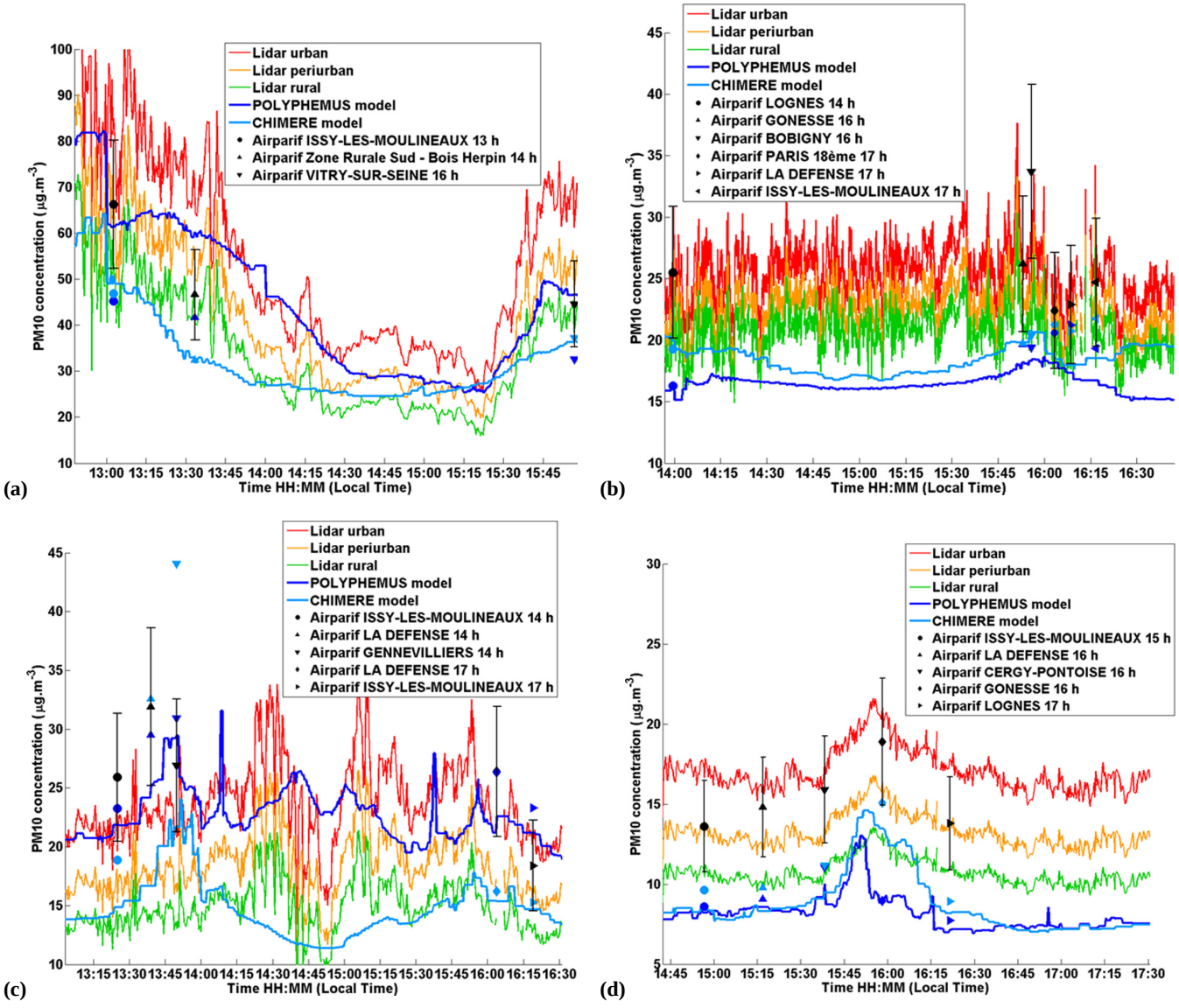

Fig. 6. Comparison for the 1 **(a)**, 15 **(b)**, 16 **(c)** and 26 **(d)** July of wet PM_{10} derived from GBML using urban (red curves), peri-urban (orange) and rural relationships (green) at 210 m height, and wet PM_{10} extracted from POLYPHEMUS model at 210 m height (in dark blue) and CHIMERE model at 250 m height (in light blue). AIPARIF dry PM_{10} are indicated by black symbols for the nearest stations (located at less than 10 km from GBML) and dry PM_{10} modeled at the lowest level are indicated with dark blue (for POLYPHEMUS) and light blue (for CHIMERE) filled symbols. Note that for the 15 July a mixing of dust and pollution relationships has been used in lidar inversion.

peri-urban parametrization for these comparisons. Wet PM_{10} derived from GBML using a peri-urban relationship and models have shown the following error statistics in terms of RMSE (MAPE) for POLYPHEMUS and CHIMERE (Table 6): 8.2 (13.4 %) and 13.2 $\mu g\,m^{-3}$ (24.2 %) on 1 July, 6.4 (30.7 %) and 4.8 $\mu g\,m^{-3}$ (20.3 %) on 15 July, 5.4 (22.2 %) and 5.1 $\mu g\,m^{-3}$ (24.9 %) on 16 July and 5.2 (48.3 %) and 4.7 $\mu g\,m^{-3}$ (42.4 %) on 26 July 2009. Note that on 15 July, the contribution of dust aerosol in the total PM_{10} is found to be 54.2 % (12.2 $\mu g\,m^{-3}$) with the GBML with a peri-urban relationship, which is in good agreement with CHIMERE (54 %). POLYPHEMUS under-estimates the contribution of dust aerosol on that day (31 %), because dust aerosols are probably advected from south of Europe and the boundary conditions used for the European simulation are climatological (they are not specific to July 2009). If we consider all MD, the RMSE (MAPE) between GBML with peri-urban relationship and models PM_{10} are 6.4 (29.6 %) and 6.4 $\mu g\,m^{-3}$ (27.6 %) for POLYPHEMUS and CHIMERE, respectively. As shown by the mean values for the 10 MD of 22.4, 20.0 and 17.5 $\mu g\,m^{-3}$ for GBML with a peri-urban relationship, POLYPHEMUS and CHIMERE models, respectively, both models under-estimate the wet PM_{10} concentrations.

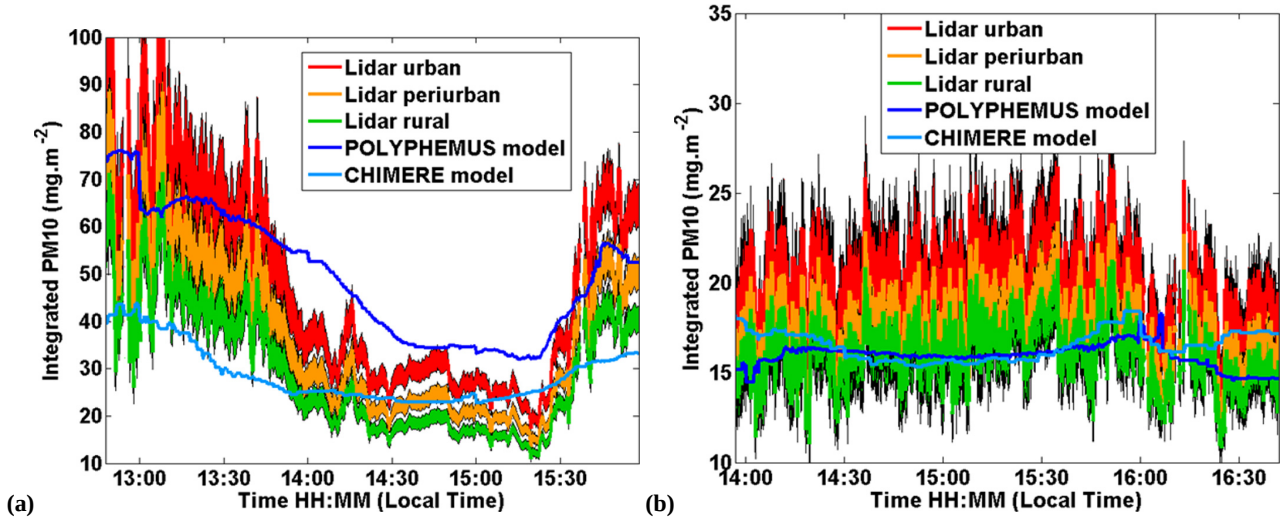

Fig. 7. Comparison for 1 **(a)** and 15 July 2009 **(b)** of wet integrated PM_{10} (between the ground and 1 km a.g.l.) derived from GBML using urban (red curves), peri-urban (orange) and rural relationships (green), and modeled with POLYPHEMUS plateform (in dark blue) and CHIMERE model (in light blue). The shaded areas on lidar integrated PM_{10} represent the uncertainty on hygroscopic effect.

5.2 Comparison between AIRPARIF ground-based measurements and modeling

Dry PM_{10} at the ground level from POLYPHEMUS and CHIMERE CTMs show a systematic underestimation (means of 20.6 and 21.4 $\mu g\,m^{-3}$, respectively) compared to AIRPARIF measurements (27.9 $\mu g\,m^{-3}$). RMSE (MAPE) are 9.1 (32.5 %) for POLYPHEMUS and 9.4 $\mu g\,m^{-3}$ (32.8 %) for CHIMERE. If AIRPARIF stations in Bobigny and Gonesse are not considered, these values drop to 7.9 $\mu g\,m^{-3}$ (29.2 %) for POLYPHEMUS and 8.7 $\mu g\,m^{-3}$ (32.9 %) for CHIMERE.

5.3 Comparison between lidar and models in term of integrated PM_{10}

Wet integrated PM_{10} has been computed between the ground level and 1 km a.g.l. for lidar, POLYPHEMUS and CHIMERE models. The top of the PBL has been deliberately excluded from the analysis to avoid an increase of RH and the presence of clouds in this part of the atmosphere. The results are summarized in Table 7 and two examples of temporal evolution of integrated PM_{10} are given in Fig. 7 for the 1 (7a) and 15 July 2009 (7b). For the lidar measurement the shaded areas represent the uncertainty on hygroscopic effect considering the uncertainty on u, γ and RH values. The results are very similar to what is observed when comparing PM_{10} concentrations at ∼200 m. All comparisons (see example in Fig. 7) of wet integrated PM_{10} show the same kind of evolution than the one of PM_{10} concentration at 200 m height (Fig. 6).

Mean integrated PM_{10} are 18.2, 21.1 and 16.2 $mg\,m^{-2}$ for GBML with the peri-urban relationship, POLYPHEMUS and CHIMERE, respectively. The RMSE (and MAPE) are 6.3 $mg\,m^{-2}$ (30.1 %) and 5.2 $mg\,m^{-2}$ (22.3 %) with POLYPHEMUS and CHIMERE when comparing with lidar-peri-urban parametrization. The POLYPHEMUS model overestimates integrated PM_{10} by ∼3 $mg\,m^{-2}$ and CHIMERE model underestimates by 2 $mg\,m^{-2}$.

5.4 Comparison to previous studies

The statistical results obtained in this study have been compared to previous regional scale model/measurements comparison studies at the regional scale.

Hodzic et al. (2004) performed a comparison of lidar backscatter signals measured at SIRTA at 600 m a.g.l. during 40 mornings (between 08:00 and 11:00 UT) between October 2002 and April 2003 with the ones derived from CHIMERE simulations. Note that their approach is alternative to our's, in the sense that lidar observables are directly calculated within the model. The relative bias was −25 % and the relative RMSE was 38 %. The model underestimation was attributed to an underestimation of SOA and mineral dust, the latter not being included in the standard run. These figures are in the range of values obtained in the present study for the CHIMERE model: relative bias −23 % (−5.2 $\mu g\,m^{-3}$) and relative RMSE of 33 % when comparing with lidar with peri-urban relationship. Hodzic et al. (2005) performed a detailed comparison of CHIMERE model simulations with AIRPARIF measurements. In summer (April to September) 2003, the PM_{10} daily mean levels are fairly well predicted, for the ensemble of urban, peri-urban and rural background sites, bias was low (−2.5 $\mu g\,m^{-3}$), and MAPE was 27 %.

Tombette and Sportisse (2007) simulated PM_{10} concentrations over Paris between 1 May 2001 and 30 September 2009 with the POLYPHEMUS system. The comparison of PM_{10} concentrations to AIRPARIF measurements gave similar results to this study (RMSE of 9.5 $\mu g\,m^{-3}$ and MAPE 32 %). Roustan et al. (2011) simulated also PM_{10} concentrations over Paris for the year 2005 with the POLYPHEMUS system. The comparison to AIRPARIF measurements led to a similar RMSE (9.8 $\mu g\,m^{-3}$) as here and as in Tombette and Sportisse (2007). However, PM_{10} concentrations are overestimated in their study, probably because the measurement network for PM_{10} did not until 2005 measure a large fraction of semi-volatile PM.

The difficulties to accurately model the semi-volatile fraction of PM_{10} at the urban/regional scale is shown by the study of Sartelet et al. (2007b). They compared modeled inorganic components of $PM_{2.5}$ (main part of PM_{10} within urban area) to measurements over Tokyo for high-pollution episodes. Using the normalized mean bias factor (B_{NMBF}) and the normalized mean absolute error factor (E_{NMAEC}) as statistical indicators, they found that sulfate is well modeled with $|B_{NMBF}| < 25\,\%$ and $E_{NMAEC} < 35\,\%$, as suggested as a criterion of model performance by Yu et al. (2006) for sulfate. However, for inorganic semi-volatile components, such as ammonium and nitrate, the model performance was lower with $E_{NMAEC} < 60\,\%$.

Finally, observations made during the HOVERT campaign (HOrizontal and VERtical Transport of ozone and particulate matter) in the Berlin agglomeration between September 2001 and 2002 were compared to REM3-CALGRID simulations. Relative RMSE differences between observed and simulated urban background PM_{10} was typically around 50 % (Beekmann et al., 2007).

As a conclusion of these different studies, statistical model to observation comparison results presented in this study seem in the same order or better than those in previous urban/regional scale studies. Before 2007, the AIRPARIF measurement network did not measure a large fraction of semi-volatile PM, underestimating PM_{10} concentrations. This underestimation may explain why modeled PM_{10} concentrations over Paris were not systematically under-estimated compared to measurements in studies made for years before 2005 (e.g. Roustan et al., 2011), stressing the importance of an accurate representation of secondary aerosols in both models and measurements.

5.5 Factors influencing the PM_{10} modeled concentrations

In order to understand which parameterizations/factors influence the most the aerosols and gas-phase species concentrations, Roustan et al. (2010) performed a sensitivity study over Europe with the POLYPHEMUS system for 2001, by changing one input data set or one parameterization at one time. They did not include the sensitivity to emissions in their study. They found that the modeled PM_{10} concentrations are most sensitive to the parameterization used for vertical turbulent diffusion, and to the number of vertical levels used. Depending on the chemical components of PM_{10} studied, the concentrations are also sensitive to boundary conditions, heterogeneous reactions at the surface of particles, the modeling of aqueous chemistry and gas/particle mass transfer, and deposition for large particles.

Beyond this general model error analysis, it is interesting to try to analyze reasons for actually occurred errors. Differences between simulations and observations may be decomposed into two factors: (1) the background PM_{10} over the domain and (2) the additional build-up from Paris agglomeration. For 26 July, background PM_{10} simulated by both models is lower than the lidar derived one even when using the rural relationship (which gives the lowest values). On the contrary, the superimposed PM_{10} peak due to Paris emissions is well simulated (Fig. 6d).

5.5.1 Influence of transport and boundary conditions

For 16 July, the Paris pollution plume is heading to north north-west as confirmed for example by NO_y measurements on the French Safire ATR-42 aircraft (A. Colomb, personal communication, 2011). However, in CHIMERE simulations, the wind is heading to North-north-east, causing a direction shift in the plume. On the contrary, in 1 July, spatial gradients, in particular the shift from large values within and near the agglomeration to much lower ones about 100 km downwind, are qualitatively well depicted by both models. As said above and depicted in Fig. 3a, for this day continental transport from North-East was important and resulted in large PM_{10} values transported to Ile de France, while for the other days, air masses were mainly of maritime origin and much cleaner. This example illustrates that both uncertainties in background PM_{10}, in the position of the plume and in its strength, can affect the PM_{10} concentrations.

5.5.2 Influence of vertical mixing and turbulent diffusion

On 1 July, the low boundary layer height until midday contributed to the high concentrations observed. Both models represent well the decrease of PM_{10} concentrations at Saclay between 13:00 LT and 16:00 LT, correlated with an increase of the PBL height from 1.2 to 1.8 km. While the Fig. 4 does not show a systematic bias between the simulated and observed boundary layer height (for the example of 1 July), it illustrates that limited vertical model resolution leads to much smoother vertical PM_{10} profiles than those deduced from lidar, where a sharp transition between the convective boundary layer and free troposphere occurs. This discussion makes evident the strength of this lidar derived data set for model evaluation, because it depicts both horizontal gradients between the agglomeration, the plume, and background values,

and vertical gradients between layers affected by pollution sources and not.

5.5.3 Influence of chemical modeling of semi-volatile components

Aerosol Mass Spectrometer (AMS) and soot measurements during the MEGAPOLI summer campaign at the Golf site/Livry Gargan at the north-eastern edge of the agglomeration made evident that secondary aerosol (inorganic and organic) made up on the average about two thirds of PM1 aerosol (J. Schneider, personal communication, 2011), thus obviously secondary formation processes are important for peri-urban aerosol and even more in the plume. Furthermore, the formation of secondary organic aerosol in the urban area and plume is likely to be under-estimated, as made evident in Sciare et al. (2010) for the CHIMERE model for an urban Paris site.

From this error analysis, it becomes clear, that model to observation differences (on the average about 30 %) can be in general explained by the combined measurement uncertainties (15–30 %) and the minimal simulation uncertainty presented in Roustan et al. (2010) (30 % in summer and 20 % in winter). This simulation uncertainty also explains differences between the CHIMERE and POLYPHEMUS simulations. For both models, particular choices of physico-chemical schemes, parameterisations, numerical set-ups and input data have been made, according to Table 4, and consequently result in model to model differences which are coherent with the model uncertainties given above.

6 Conclusion

Ten intensive observation periods (MD) were performed with ground-based mobile Rayleigh-Mie lidar (GBML) around Paris during the MEGAPOLI summer campaign. Aerosol extinction profiles have been converted into mass concentrations (PM_{10}) profiles using optical-to-mass relationships (urban, peri-urban, rural and dust) previously established for the Paris area. This set of comparisons makes evident horizontal and vertical PM_{10} gradients in air masses within and outside the Paris agglomeration pollution plume and at different distances from the agglomeration. Lidar derived PM_{10} levels are compared with CHIMERE and POLYPHEMUS chemistry-transport models (CTMs) simulations and AIPARIF network ground-based measurements. These comparisons have highlighted a very good agreement between GBML and measurements from the AIRPARIF network with a RMSE (MAPE) of 7.2 $\mu g\,m^{-3}$ (26.0 %) and 8.8 $\mu g\,m^{-3}$ (25.2 %) for peri-urban and urban parametrizations (where most of the comparisons have been realized). This value is close to the expected uncertainty of this method. For each MD the pollution plume has been sampled and can be clearly identified from GBML measurements. Lidar measurements give informations on the vertical repartition of aerosols concentration in the atmospheric contrary to in-situ ground-based measurements. The use of a N_2-Raman lidar, measuring extinction-to-backscatter profiles during both daytime and nighttime and in presence of high clouds, could significantly improve the retrieval of PM_{10} from a ground-based lidar. The comparisons between lidar-derived PM_{10} with peri-urban relationship and CTMs within the low PBL have shown a RMSE (MAPE) of 6.4 (29.6 %) and 6.4 $\mu g\,m^{-3}$ (27.6 %) for POLYPHEMUS and CHIMERE models, respectively. These differences are partly due to an underestimation of wet PM_{10} as revealed by the mean values for the 10 MD of 22.4, 20.0 and 17.5 $\mu g\,m^{-3}$ for GBML with a peri-urban relationship, POLYPHEMUS and CHIMERE models, respectively. Similar differences have been computed for the integrated PM_{10} within the PBL (RMSE of 6.3 $mg\,m^{-2}$ (30.1 %) and 5.2 $mg\,m^{-2}$ (22.3 %) for POLYPHEMUS and CHIMERE models, respectively). When comparing dry PM_{10} at ground level from AIRPARIF ground-based measurements to CTMs simulation RMSE (MAPE) is 9.1 $\mu g\,m^{-3}$ (32.5 %) with POLYPHEMUS and 9.4 $\mu g\,m^{-3}$ (32.8 %) with CHIMERE. The discrepancies observed between models and measured PM_{10} can be explained by difficulties to accurately model background conditions, represent model transport (positions and strengths of the plume), limited vertical model resolutions and chemical modeling such as the formation of secondary aerosols. On the whole, model to observation differences are coherent with the error budgets of both observations and simulations and are of the same order of magnitude than comparisons realized in previous studies.

This is one of the first papers presenting results of the MEGAPOLI Paris campaigns. Forthcoming papers will present more detailed results about the comparison of lidar-derived PM_{10} measurements with aircraft observations and about model evaluation with chemically resolved aerosol measurements.

Acknowledgements. The research leading to these results has received funding from the European Union's Seventh Framework Programme FP/2007-2011 under grant agreement no. 212520. This work has been supported by the Commissariat à l'Energie Atomique (CEA). The authors would like to thank AIRPARIF and AERONET network for collecting and providing data around Paris and SIRTA site for providing ALS450 Rayleigh-Mie lidar data used in this study. CHIMERE modelling results have been obtained under Ph-D grant funding by CIFRE (ANRT) attributed to ARIA Technologies and LISA.

Edited by: A. Baklanov

The publication of this article is financed by CNRS-INSU.

References

Angström, A.: The parameters of atmospheric turbidity, Tellus, 16, 64–75, 1964.

Aumont, B., Chervier, F., and Laval, S.: Contribution of HONO to the NOx/HOx/O3 chemistry in the polluted boundary layer, Atmos. Environ., 37, 487–498, 2003.

Beekmann, M. and Derognat, C.: Monte Carlo Uncertainty analysis of a regional sale transport chemistry model constrained by measurements from the ESQUIF campaign, J. Geophys. Res., 108., 8559, doi:10.1029/2003JD003391, 2003.

Beekmann, M. and Vautard, R.: A modelling study of photochemical regimes over Europe: robustness and variability, Atmos. Chem. Phys., 10, 10067–10084, doi:10.5194/acp-10-10067-2010, 2010.

Beekmann, M., Kerschbaumer, A., Reimer, E., Stern, R., and Möller, D.: PM measurement campaign HOVERT in the Greater Berlin area: model evaluation with chemically specified particulate matter observations for a one year period, Atmos. Chem. Phys., 7, 55–68, doi:10.5194/acp-7-55-2007, 2007.

Bessagnet, B., Hodzic, A., Vautard, R., Beekmann, M., Cheinet, S., Honoré, C., Liousse, C., and Rouil, L.: Aerosol modeling with CHIMERE-preliminary evaluation at the continental scale, Atmos. Environ., 38, 2803–2817, 2004.

Bessagnet, B., Hodzic, A., Blanchard, O., Lattuati, M., Le Bihan, O., Marfaing, H., and Rouil, L.: Origin of particulate matter pollution episodes in wintertime over the Paris basin, Atmos. Environ., 39, 6159–6174, 2005.

Bessagnet, B., Menut, L., Curci, G., Hodzic, A., Guillaume, B., Liousse, C., Moukhtar, S., Pun, B., Seigneur C., and Schulz, M.: Regional modeling of carbonaceous aerosols over Europe – focus on secondary organic aerosols, J. Atmos. Chem., 61, 175–202, 2008.

Chazette, P.: The monsoon aerosol extinction properties at Goa during INDOEX as measured with lidar, J. Geophys. Res., 108, 4187, doi:10.1029/2002JD002074, 2003.

Chazette, P., Randriamiarisoa, H., Sanak, J., Couvert P., and Flamant, C.: Optical properties of urban aerosol from airborne and ground-based in situ measurements performed during the ESQUIF program, J. Geophys. Res., 110, D02206, doi:10.1029/2004JD004810, 2005.

Chazette, P., Sanak, J., and Dulac, F.: New Approach for Aerosol Profiling with a Lidar Onboard an Ultralight Aircraft: Application to the African Monsoon Multidisciplinary Analysis, Environ. Sci. Technol., 41, 8335–8341, 2007.

Debry, E., Fahey, K., Sartelet, K., Sportisse, B., and Tombette, M.: Technical Note: A new SIze REsolved Aerosol Model (SIREAM), Atmos. Chem. Phys., 7, 1537–1547, doi:10.5194/acp-7-1537-2007, 2007.

Deguillaume, L., Beekmann, M, and Menut, L.: Bayesian Monte Carlo analysis applied to regional scale inverse emission modelling for reactive trace gases, J. Geophys. Res., 112, D02307, doi:10.1029/2006JD007518, 2007.

Deguillaume, L., Beekmann, M., and Derognat, C.: Uncertainty evaluation of ozone production and its sensitivity to emission changes over the Ile-de-France region during summer periods, J. Geophys. Res., 113, D02304, doi:10.1029/2007JD009081, 2008.

De Moore, W. B., Sandetr, S. P., Golden, D. M., Hampton, R. F., Kurylo, M. J., Howard, C. J., Ravishankara, A. R., Kolb, C. E., and Molina, M. J.: Chemicla kinetics and photochemical data for use in stratospheric modeling evaluation, JPL publication, 94, 26, JPL, Pasadena, US, 1994.

Derognat, C., Beekmann, M., Bäumle, M., Martin, D., and Schmidt, H.: Effect of biogenic volatile organic compound emissions on the tropospheric chemistry during elevated ozone periods in Ile de France, J. Geophys. Res., 108, 8560, doi:10.1029/2001JD001421, 2003.

Dockery, D. and Pope, A.: Epidemiology of acute health effects: summary of time-series, in: Particles in Our Air: Concentration and Health Effects, edited by: Wilson, R. and Spengler, J. D., Harvard University Press, Cambridge, MA, USA, 123–147, 1996.

Dudhia, J.: A nonhydrostatic version of the Penn state NCAR mesoscale model – validation tests and simulation of an atlantic cyclone and cold-front, Mon. Weather Rev., 121, 1493–1513, 1993.

Elias, T., Haeffelin, M., Drobinski, P., Gomes, L., Rangognio, J., Bergot, T., Chazette, P., Raut, J.-C., and Coulomb, M.: Particulate contribution to extinction of visible radiation: pollution, haze, and fog, Atmos. Res., 92, 443–454, doi:10.1016/j.atmosres.2009.01.006, 2009.

Fahey, K. M. and Pandis, S. N.: Optimizing model performance: variable size resolution in cloud chemistry modeling, Atmos. Environ., 35, 4471–4478, 2001.

Guenther, A., Karl, T., Harley, P., Wiedinmyer, C., Palmer, P. I., and Geron, C.: Estimates of global terrestrial isoprene emissions using MEGAN (Model of Emissions of Gases and Aerosols from Nature), Atmos. Chem. Phys., 6, 3181–3210, doi:10.5194/acp-6-3181-2006, 2006.

Gurjar, B. R., Butler, T. M., Lawrence, M. G., and Lelieveld, J.: Evaluation of Emissions and Air Quality in Megacities, Atmos. Environ., 42, 1593–1606, doi:10.1016/j.atmosenv.2007.10.048, 2008.

Haeffelin, M., Bergot, T., Elias, T., Tardif, R., Carrer, D., Chazette, P., Colomb, M., Drobinski, P., Dupont, E., Dupont, J.-C., Gomes, L., Musson-Genon, L., Pietras, C., Plana-Fattori, A., Protat, A., Rangognio, J., Raut, J.-C., Rémy, S., Richard, D., Sciare, J., and Zhang, X.: ParisFog, shedding new light on fog physical processes, B. Am. Meteorol. Soc., 91, 767–783, doi:10.1175/2009BAMS2671.1, 2010.

Hänel, G.: The properties of atmospheric aerosol particles as functions of the Relative humidity at thermodynamic equilibrium with the surrounding moist air, Adv. Geophys., 19, 73–188, 1976.

Hauglustaine, D. A., Hourdin, F., Jourdain, L., Filiberti, M.-A., Walters, S., Lamarque, J.-F., and Holland, E. A.: Interactive chemistry in the Laboratoire de Météorologie Dynamique general circulation model: Description and background tropospheric chemistry evaluation, J. Geophys. Res., 109, D04314, doi:10.1029/2003JD003957, 2004.

Hodzic, A., Chepfer, H., Chazette, P., Beekmann, M., Bessagnet, B., Drobinski, P., Goloub, P., Haeffelin, M., Morille, Y., and Vautard, R.: Comparison of aerosol chemistry-transport model simulations with lidar and sun-photometer observations at a site near Paris, J. Geophys. Res., 109, D23201, doi:10.1029/2004JD004735, 2004.

Hodzic, A., Vautard, R., Bessagnet, B., Lattuati, M., and Moreto, F.: Long-term urban aerosol simulation versus routine particulate matter observations, Atmos. Environ., 39, 5851–5864, 2005.

Holben, B. N., Eck, T. F., Slutsker, I., Tanré, D., Buis, J. P., Setzer, A., Vermote, E., Reagan, J. A., Kaufman, Y., Nakajima, T., Lavenu, F., Jankowiak, I., and Smirnov, A.: AERONET – A federated instrument network and data archive for aerosol characterization., Rem. Sens. Environ., 66, 1–16, 1998.

Honoré, C., Rouïl, L., Vautard, R., Beekmann, M., Bessagnet, B., Dufour, A., Elichegaray, C., Flaud, J.-M., Malherbe, L., Meleux, F., Menut, L., Martin, D., Peuch, A., Peuch, V. H., and Poisson, N.: Predictability of European air quality: The assessment of three years of operational forecasts and analyses by the PREV'AIR system, J. Geophys. Res., 113, D04301, doi:10.1029/2007JD008761, 2008.

Jacob, D. J.: Heterogeneous chemistry and tropospheric ozone, Atmos. Environ, 34, 2131–2159, 2000.

Junker, C. and Liousse, C.: A global emission inventory of carbonaceous aerosol from historic records of fossil fuel and biofuel consumption for the period 1860–1997, Atmos. Chem. Phys., 8, 1195–1207, doi:10.5194/acp-8-1195-2008, 2008.

Klett, J. D.: Lidar inversion with variable backscatter/extinction ratios, Appl. Optics, 24, 1638–1643, 1985.

Kim, Y., Couvidat, F., Sartelet, K., and Seigneur, C.: Comparison of different gas-phase mechanisms and aerosol modules for simulating particulate matter formation, J. Air Waste Manage. Assoc., in press, 2011a.

Kim, Y., Sartelet, K., and Seigneur, C.: Formation of secondary aerosols over Europe: comparison of two gas-phase chemical mechanisms, Atmos. Chem. Phys., 11, 583–598, doi:10.5194/acp-11-583-2011, 2011b.

Konovalov, I. B., Beekmann, M., Richter, A., and Burrows, J. P.: Inverse modelling of the spatial distribution of NO_x emissions on a continental scale using satellite data, Atmos. Chem. Phys., 6, 1747–1770, doi:10.5194/acp-6-1747-2006, 2006.

Lavigne, C., Roblin, A., Chervet, P., and Chazette, P.: Experimental and theoretical studies of the aureole about a point source that is due to atmospheric scattering in the middle ultraviolet, Appl. Optics, 44, 1250–1262, doi:10.1364/AO.44.001250, 2005.

Lauwerys, R. R.: Toxicologie industrielle et intoxications professionnelles, Masson, 1982.

Lawrence, M. G., Butler, T. M., Steinkamp, J., Gurjar, B. R., and Lelieveld, J.: Regional pollution potentials of megacities and other major population centers, Atmos. Chem. Phys., 7, 3969–3987, doi:10.5194/acp-7-3969-2007, 2007.

Nenes, A., Pilinis, C., and Pandis, S.: ISORROPIA: A new thermodynamic equilibrium model for multicomponent inorganic aerosols, Aquat. Geochem., 4, 123–152, 1998.

Pataschnik, H. and Rupprecht, E. G.: Continuous PM10 measurements using a tapered element oscillating microbalance, J. Air and Waste Manag. Assoc., 41, 1079–1083, 1991.

Pun, B. K., Griffin, R. J., Seigneur, C., and Seinfeld, J. H.: Secondary organic aerosol 2. Thermodynamic model for gas/particle partitioning of molecular constituents, J. Geophys. Res., 107, 4333, doi:10.1029/2001JD000542, 2002.

Pun, B., Seigneur, C., and Lohman, K.: Modeling secondary organic aerosol via multiphase partitioning with molecular data, Environ. Sci. Technol., 40, 4722–4731, 2006.

Randriamiarisoa, H., Chazette, P., Couvert, P., Sanak, J., and Mégie, G.: Relative humidity impact on aerosol parameters in a Paris suburban area, Atmos. Chem. Phys., 6, 1389–1407, doi:10.5194/acp-6-1389-2006, 2006.

Raut, J.-C. and Chazette, P.: Retrieval of aerosol complex refractive index from a synergy between lidar, sunphotometer and in situ measurements during LISAIR experiment, Atmos. Chem. Phys., 7, 2797–2815, doi:10.5194/acp-7-2797-2007, 2007.

Raut, J.-C. and Chazette, P.: Assessment of vertically-resolved PM_{10} from mobile lidar observations, Atmos. Chem. Phys., 9, 8617–8638, doi:10.5194/acp-9-8617-2009, 2009.

Raut, J.-C., Chazette, P., and Fortain, A.: New approach using lidar measurements to characterize spatiotemporal aerosol mass distribution in an underground railway station in Paris, Atmos. Environ., 43, 575–583, doi:10.1016/j.atmosenv.2008.10.002, 2009a.

Raut, J.-C., Chazette, P., and Fortain, A.: Link between aerosol optical, microphysical and chemical measurements in an underground railway station in Paris, Atmos. Environ., 43, 860–868, doi:10.1016/j.atmosenv.2008.10.002, 2009b.

Rouil, L., Honoré, C., Vautard, R., Beekman, M., Bessagnet, B., Malherbe, L., Meleux, F., Dufour, A., Elichegaray, C., Flaud, J.-M., Menut, L., Martin, D., Peuch, V.-H., and Poisson, N.: PREV'AIR: an operational forecasting and mapping system for air quality in Europe, B. Am. Meteorol. Soc., 90, 73, doi:10.1175/2008BAMS2390.1, 2009.

Roustan, Y., Sartelet, K. N., Tombette, M., Debry, É., and Sportisse, B.: Simulation of aerosols and gas-phase species over Europe with the POLYPHEMUS system. Part II: Model sensitivity analysis for 2001, Atmos. Environ., 41, 6116–6131, doi:10.1016/j.atmosenv.2010.07.005, 2010.

Roustan, Y., Pausader, M., and Seigneur, C.: Estimating the effect of on-road vehicle emission controls on future air quality in Paris, France, Atmos. Environ., in press, doi:10.1016/j.atmosenv.2010.10.010, 2011.

Royer, P., Chazette, P., Lardier, M., and Sauvage, L.: Aerosol content survey by mini N2-Raman lidar: Application to local and long-range transport aerosols, Atmos. Environ., in press, 2011.

Sartelet, K., Debry, E., Fahey, K., Roustan, Y., Tombette, M., and Sportisse, B.: Simulation of aerosols and gas-phase species over Europe with the Polyphemus system. Part I: model-to-data comparison for 2001, Atmos. Environ., 41, 6116–6131, doi:10.1016/j.atmosenv.2007.04.024, 2007a.

Sartelet, K., Hayami, H., and Sportisse, B.: Dominant aerosol processes during high-pollution episodes over Greater Tokyo, J. Geophys. Res., 112, D14214, doi:10.1029/2006JD007885, 2007b.

Sartelet, K., Hayami, H., and Sportisse, B.: MICS Asia Phase II Sensitivity to the aerosol module, Atmos. Environ., 42, 3562–3570, doi:10.1016/j.atmosenv.2007.03.05, 2008.

Schmidt, H., Derognat, C., Vautard, R., and Beekmann, M.: A comparison of simulated and observed ozone mixing ratios for summer of 1998 in western Europe, Atmos. Environ., 35, 6277–6297, 2001.

Sciare, J., d'Argouges, O., Zhang, Q. J., Sarda-Estève, R., Gaimoz, C., Gros, V., Beekmann, M., and Sanchez, O.: Comparison between simulated and observed chemical composition of fine aerosols in Paris (France) during springtime: contribution of regional versus continental emissions, Atmos. Chem. Phys., 10, 11987–12004, doi:10.5194/acp-10-11987-2010, 2010.

Seinfeld, J. H. and Pandis, S. N.: Atmospheric chemistry and physics: From air pollution to climate change, Wiley-Interscience, 1997.

Simpson, D., Winiwarter, W., Börjesson, G., Cinderby, S., Rerreiro,

A., Guenther, A., Hewitt, C. N., Janson, R., Khalil, M. A. K., Owen, S., Pierce, T. E., Puxbaum, H., Shearer, M., Skiba, Ute, Steinbrecher, R., Tarrasón, L., and Öquist, M. G.: Inventorying emissions from nature in Europe, J. Geophys. Res., 104, 8113–8152, doi:10.1029/98JD02747, 1999.

Stockwell, W. R., Kirchner, F., Kuhn, M., and Seefeld, S.: A new mechanism for regional atmospheric chemistry modeling, J. Geophys. Res., 102, 25847–25879, 1997.

Tombette, M. and Sportisse, B.: Aerosol modeling at a regional scale: Model-to-data comparison and sensitivity analysis over Greater Paris, Atmos. Environ., 41, 6941–6950, 2007.

Tombette, M., Chazette, P., Sportisse, B., and Roustan, Y.: Simulation of aerosol optical properties over Europe with a 3-D size-resolved aerosol model: comparisons with AERONET data, Atmos. Chem. Phys., 8, 7115–7132, doi:10.5194/acp-8-7115-2008, 2008.

Troen, I. B. and Mahrt, L: A simple model of the atmospheric boundary layer; sensitivity to surface evaporation, Bound.-Layer Meteorol., 37, 129–148, 1986.

Vautard, R., Beekmann, M., Roux, J., and Gombert, D.: Validation of a hybrid forecasting system for the ozone concentrations over the Paris region, Atmos. Environ., 35, 2449–2461, 2001.

Vautard, R., Menut, L., Beekmann, M., Chazette, P., Flamant, P. H., Gombert, D., Guédalia, D., Kley, D., Lefebvre, M.-P., Martin, D., Mégie, G., Perros P., and Toupance, G.: A synthesis of the Air Pollution Over the Paris Region (ESQUIF) field campaign, J. Geophys. Res., 108, 8558, doi:10.1029/2003JD003380, 2003.

Yu, S., Eder, B., Dennis, R., Chu, A.-H., and Schwartz, S.H.: New unbiased symmetric metrics for evaluation of air quality models, Atmos. Sci. Lett., 7, 26–34, 2006.